



HAL
open science

Good practices for designing and experimental testing of dynamically excited jointed structures: The Orion beam

Rafael Teloli, Pauline Butaud, Gael Chevallier, Samuel da Silva

► To cite this version:

Rafael Teloli, Pauline Butaud, Gael Chevallier, Samuel da Silva. Good practices for designing and experimental testing of dynamically excited jointed structures: The Orion beam. *Mechanical Systems and Signal Processing*, 2022, 163, pp.108172 (23). hal-03692998

HAL Id: hal-03692998

<https://hal.science/hal-03692998>

Submitted on 10 Jun 2022

HAL is a multi-disciplinary open access archive for the deposit and dissemination of scientific research documents, whether they are published or not. The documents may come from teaching and research institutions in France or abroad, or from public or private research centers.

L'archive ouverte pluridisciplinaire **HAL**, est destinée au dépôt et à la diffusion de documents scientifiques de niveau recherche, publiés ou non, émanant des établissements d'enseignement et de recherche français ou étrangers, des laboratoires publics ou privés.

Good practices for designing and experimental testing of dynamically excited jointed structures: the Orion beam

Rafael de O. Teloli ¹, Pauline Butaud ², Gaël Chevallier ², Samuel da Silva ¹

¹ UNESP - Universidade Estadual Paulista, Faculdade de Engenharia de Ilha Solteira,
5 Departamento de Engenharia Mecânica, Av. Brasil, 56, Ilha Solteira, 15385-000, SP,
Brasil

² Univ. Bourgogne Franche-Comté, FEMTO-ST Institute,
CNRS/UFC/ENSMM/UTBM, Department of Applied Mechanics, 24 chemin de
l'Épitaphe, 25000 Besançon, France

10 corresponding authors: ¹rafael.teloli@gmail.com and ²gael.chevallier@univ-fcomte.fr

Abstract

This paper proposes a new lap-joint configuration, the so-called Orion beam. The new setup is composed of two thin beams connected by three bolted joints with contact patches on each connecting bolt. The Orion beam suggests an assembly configuration. There are bolts dedicated to “static” functions to guarantee structural integrity and those that perform “damping” functions to increase energy dissipation due to frictional contact. In particular, this paper analyzes the influence of the Orion beam’s design in the repeatability of experimental measurements and the impact of the tightening torque and excitation amplitudes on the system’s response. A feedback controller is proposed to control the excitation amplitudes during step-sine tests in the vicinity of resonance frequencies to measure the frequency response curves used to perform such analysis. Additionally, a single-degree-of-freedom Duffing-Van der Pol oscillator is proposed to evaluate, through its calibrated parameters, the impact of several tightening torque conditions and multiple excitation amplitudes on the structural stiffness and damping considering the vibration mode that promotes pronounced deformation around the lap-joint. Due to the presence of contact patches, the results show that the structure maintained impressive repeatability after several experimental measurements. Besides, it is possible to increase the damping for amplitude attenuation without significant losses in the contact stiffness.

Keywords: lap-joint, tightening torque, experimental practices, nonlinear dynamics, contact mechanics, friction damping

1. INTRODUCTION

15 Engineering structures are built with assembled components, with appli-
cations ranging from the energy industries to aeronautics [1, 2]. Nonetheless,
understanding jointed structures' behavior remains challenging since these
structures behave with very complex nonlinearities that appear from con-
tact interfaces. The nonlinear features are mainly related to frictional ef-
fects from the microscopic relative motion between the contacting bodies.
20 Such micro-scale tribology leads at the vibration scale to generalized forces,
which contains hysteretic and softening effects. In the experimental or nu-
merical observations, this induces the decreasing of the resonant frequencies
according to vibrational amplitudes and considerable sensitivity to contact
pressure [3, 4, 5]. The scientific community investigating the dynamics of
25 joint structures, which is very active, contributes to measurement, modeling,
and designing. M. Brake's book (2018) [6] illustrates contributions in these
different fields. This current article contributes to the aspects related to the
measurement and design of damping links.

30 Three issues must be considered for designing an assembly setup: the
architecture, the physical constraints of setup configurations, and the exci-
tation device.

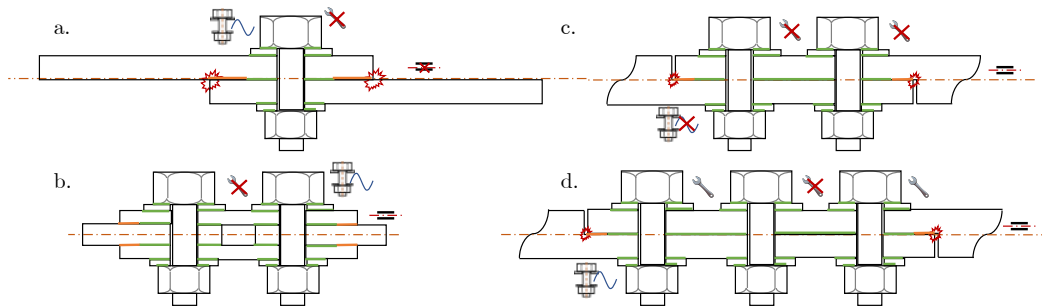


Figure 1: Schemes of several bolted joints. (a) Single bolted joint [7, 8]; (b) Full symmetric double bolted joint [9]; (c) Double bolted joints [10, 11];(d) Brake-Reuß beam (BRB), three bolted connections [12]. Details about the pictograms are available in Appendix A.

Many benchmarks have been studied from the testing and the modeling point of view, considering different possible architectures. Figures 1 and 2 summarize the main configurations using pictograms, which are defined in the Appendix A, to highlight their properties. Ahmadian and Jalali (2007) [7, 8] proposed a simple assembly illustrated in Fig. 1(a), which is composed of two beams and a single bolted connection. This setup is supposed to be the simplest one, but due to a single bolt and the lack of structural symmetry, dynamic clearance may occur between interfaces. These effects lead to quite complex dynamics that are not representative of well-designed assemblies. The drawbacks involving this setup design have been (partially) circumvented by Festjens et al. (2011), who proposed the configuration illustrated in Fig. 1(c) [11]. The authors proposed a two bolts assembly with better structural symmetry that allows minimizing parasitic clearance. Later, Jalali et al. (2019) [10] showed that such configurations ((a) and (c)) are quite sensitive to shape uncertainties and roughness, especially at the low-pressure contact areas, represented by orange lines in Fig. 1. Song (2004) [9] proposed a full symmetric setup that minimizes dynamic clearance and uncertainties due to surface imperfections, as presented in Fig. 1(b). Brake et al. (2014) [12] have introduced the Brake-Reuß beam (BRB), a 2-thick-beams assembly with three bolts at its center, as seen in Fig. 1(d). Several research groups have tested this well-known setup and has been derived in various versions considering different contact shapes. In our opinion, the BRB's main improvement compared to previous setups lies in the possibility of decreasing the tightening torque in the three bolts to increase the damping without loss of stiffness. Additionally, due to the beam thickness, the setup is significantly sensitive to contact imperfections once the contact stiffness strongly depends on the volume stiffness. Due to this characteristic, the BRB is representative of a specific class of assembly. Finally, Peyret et al. (2010) [13] and Dion et al. (2013) [14] proposed the clamped-clamped beam, which is depicted in Fig. 2, for experimental characterization of the damping induced by friction and partial slip on a planar transverse interface. The setup enables us to perfectly fit the friction effects with Masing's assumptions as there is no coupling between the normal load and the tangential load in such a configuration. The setup is fully symmetric and allows tunability of the normal load.

Still, other benchmarks in literature contribute to the characterization of nonlinear behavior in assembled structures and provide experimental data assessing numerical models. For example, one may see the S-4 Beam pro-

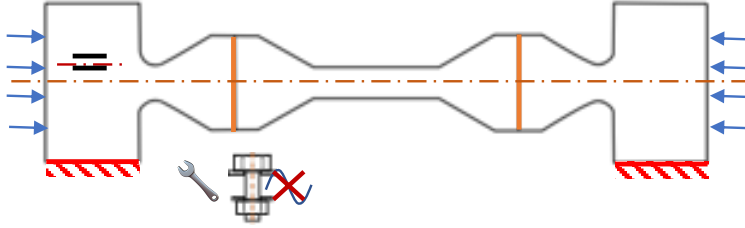


Figure 2: Clamped-clamped beam with transverse interfaces [13, 14]. Details about the pictograms are available in Appendix A.

posed by Singh et al. (2019) [15], in which the assembly consists of two C-shaped beams bolted together at their extremities. The test setup presents remarkable nonlinearity in its damping, but due to its design, the joints can experience breathing effects (dynamic clearance) depending on the mode shape. More recently, M. Scheel et al. (2020) [16] proposed a new design for lap-joint structures, which is composed of a cantilever beam that permits to vary the joint's position to study different setup configurations and severeness of nonlinearity. The specimen presents a strong influence of dry friction effects, with a significant increase of modal damping and decreasing in resonant frequencies.

It should be stressed that the objective herein is to determine the evolution of the resonance frequency and damping according to the amplitude of the solicitations, the so-called “modal backbone” (see Peyret et al. (2016) [17]). To achieve this goal, one must try to excite only one vibration mode at a time and cover a wide range of amplitudes. First of all, the boundary conditions applied to the structure make it possible to stress the joint with more or less amplitude. Three sets of boundary conditions are found in the literature; see Fig. 3 (a)-(c). The simplest testing conditions are the free-free conditions fully inspired by linear modal analysis, see [9, 12, 10]. This boundary condition avoids parasitic effects, such as added damping or lack of rigidity that comes from boundary conditions. Unfortunately, the free-free condition does not allow the testing structure to reach large vibration magnitudes. The second classical way is to work in clamped-clamped or clamped-free conditions [11, 13, 14, 17], as illustrated in Fig. 3(b). Unlike the free-free case, these boundary conditions can reach large vibration magnitudes, which is fundamental to characterize the nonlinearity. Nonetheless, the clamp design must be carried out carefully; see section 2.2. One last alternative is to connect inertia to the ends of the specimen to increase the

loading of the joint even in free-free conditions, as illustrated in Fig. 3(c).
 100 L. Gaul has suggested this alternative (1997) [18] and explored again by M. Scheel et al. (2018) [19]. This boundary is a simple way of loading the joints, but, in contrast, it is technologically more difficult to design since the added weights can generate parasitic preloads.

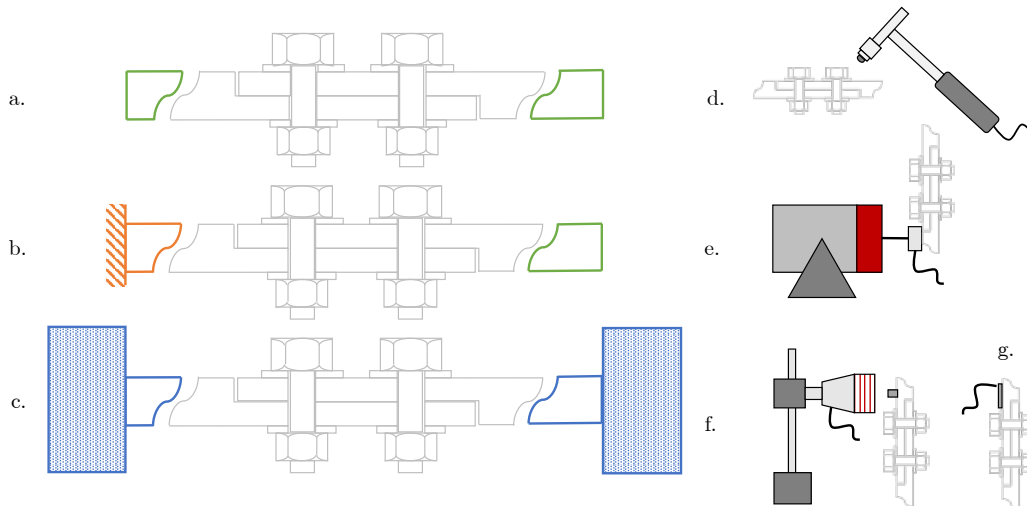


Figure 3: Schematic representation of different types of setup. (a) bolted joint in free-free conditions [9, 12, 10]; (b) bolted joint in clamped-clamped or clamped-free conditions [11, 13, 14, 17]; (c) bolted joint with inertial loadings [18];(d) Impact hammer;(e) Vibration shaker; (f) Voice coil; (g) Piezoelectric device.

To achieve the measurement of frequency response functions (FRFs) or to
 105 achieve backbone tracking, it is necessary to use a proper excitation device. In linear modal analysis, the most popular devices are impact hammers [12], see Fig. 3(d). No permanent connection with the structure is the main advantage of these excitation devices. Unfortunately, the vibration signal they generate has a high-frequency content and a low amplitude of excitation. Vi-
 110 bration shakers (Fig. 3(e)) are adequate (tools) to obtain a very controlled frequency content and higher magnitudes [19]. The main drawback is that this device changes the dynamics of the structures due to its impedance. It is interesting to point out that some works are trying to propose exotic excitation devices such as coils or piezoelectric devices to couple the advantages
 115 of both hammers and shakers [17].

Vibration reduction is an old-fashioned topic, Depending on the phenomena intended to highlight, the designing choices are not the same. Many

researchers worked and are still working on polymers, active devices, tuned mass dampers, or meta-materials to mitigate vibrations. Notwithstanding, there is also a need to search for solutions that use joints' inevitable presence in built-up structures. Optimizing the lap-joints design for enhanced vibration attenuation purposes also represents a cost reduction since it lowers the need for using exogenous solutions to the structure. However, from the designing point of view, many issues remain open. First of all, to assess experimentally the performances for which the structure has been designed, it is mandatory to reduce uncertainties. The latter generally comes from shape imperfections and dynamic clearance, as seen in Fig. 1.

It is difficult to achieve high damping and stiffness simultaneously. For damping, low contact pressures are required, whereas the bolted joints must provide the structure of increased resistance to static and dynamic loads and avoid loosening torque at the bolt connection. The main variables to guarantee these objectives may be summarized as interface positions, bolts diameter, and the tightening torque. Thus, to generate damping from frictional effects in bolted joint structures, the connections' requirements must generally be modified. For instance, if on the one hand conditions in which a low tightening torque is applied may lead to higher frictional energy dissipation [6], on the other hand, the structural integrity may be compromised.

In this context, this work introduces a new lap-joint configuration, so-called "Orion beam"¹, aiming both to provide experimental data for modeling and design purposes. In this new assembly design, 2-thin-beams are assembly by three bolts that are playing different structural functions. Contact patches have been added at each bolt connection to retain the contact between both beams in a small area, minimizing uncertainties on the structure's response and enhancing the repeatability between measurements. The central bolt is dedicated to "static" functions to ensure structural integrity and provide resistance to dynamic loads without substantial stiffness changes. The external bolts, in turn, perform "damping" functions to increase energy dissipation due to frictional contact, in which the torque preload can be set without changing the nominal frequency. Thus, the Orion beam presents the benefit of amplitude attenuation without significant losses in the contact

¹The name "Orion beam" derives from the Orion constellation, in which four stars are forming a roughly rectangular shape are linked in the center by three stars that form Orion's belt, similar to the three bolts proposed by the lap-joint configuration.

stiffness, which paves the way for proposing new control techniques in jointed structures by combining vibration amplitude attenuation and bolt preload. Preliminary investigations on vibration reduction by control of tightening load were addressed by Bouaziz et al. (2016) [20], but there is still a lack of
155 contributions in the literature that needs to be addressed.

Additionally, this work also shares with readers all the numerical and experimental data presented during this study and discussion. Moreover: the geometrical step, the numerical mesh, and all the experimental measurements performed on our lap-joint for several excitation amplitudes and
160 tightening torques, as far as possible and with the degree of uncertainties of the measures, are open access. By doing so, we intend to provide experimental data, as precise and reliable as possible, which are required to progress on the numerical modeling of the dry friction damping in assembly structures.

The paper is organized into 5 sections. First, section 2 introduces the
165 Orion beam's design, the experimental setup, and considerations regarding experimental measurements. Section 3 presents a complete description of the real-time feedback controller designed for this work to control the excitation force as frequency changes during step-sine tests to overcome limitations regarding amplitude control. Next, section 4 presents the experimental results
170 of the Orion beam around the vibrating mode most affected by the presence of nonlinearities, discussing the repeatability of measurements, influences of the tightening torque, and impact of several excitation amplitudes on the structure behavior based on a single-point measurement. Based on single-point measurements, a single-degree-of-freedom (SDoF) Duffing-Van der Pol
175 oscillator is introduced to fit the characteristics present in the frequency response curves of the lap-joint structure around the vibrating mode of interest. Finally, section 5 reports the final remarks, expected contributions of the Orion beam for the joint structures' community, and proposes the next steps for future work.

180 2. STRUCTURE DESIGN

Recently, the discussion about how the tightening torque influences the system's response has been addressed in a lap-joint configuration similar to Fig. 1(c). The study carried out by Jalali et al. (2019) [10] showed that, for the modes most affected by the lap-joint presence, the changes
185 on the bolt preload leads to changes in the contact stiffness. This section starts presenting the Orion beam's design to minimize the effects that the tightening torque has on contact stiffness and, at the same time, to maximize

the damping effects due to friction dissipation. The experimental setup, experimental protocol, and vibration sense are also addressed.

190 *2.1. The Orion beam*

The idea behind the new lap-joint configuration lies in highlighting the damping that results from friction effects, which are retained on the contact interface rather than stiffness changes. The lap-joint consists of two assembly duraluminium beams with dimensions of $200 \times 30 \times 2$ [mm] and connected by three M4 bolts spaced along a length 30 mm, as depicted in Fig. 4. A washer is placed under each screw and nut. There are contact patches at each bolt connection to retain the contact between both beams in a small area. These patches consist of a square of 12×12 mm with an extra thickness of 1 mm. To minimize the presence of residual stresses due to the manufacturing process, which may induce stress-stiffening alterations as a result of internal loads, the beams were manufactured using the electrical discharge machining (EDM) process, providing mechanical precision on the components without any distortions. The thinner design enhances the conformability of the jointed interface and provides more superior repeatability of the measurements if the experiment is appropriately controlled (see Section 4.2.2). The Orion beam suggests an assembly configuration that associates bolts dedicated to “static” functions and those performing “damping” functions. This ensures a significant increase in the structural damping without degrading the structural stiffness.

210 The central bolt’s preload is maintained, ensuring the appropriately tighten condition and then warranting its static function. In contrast, the tightening torque of the external bolts is variable for each testing condition to examine its influence on the structure’s response. Figure 4(b) represents the patches after the experimental testing campaign. Note that there exist black traces on the external patch. From this qualitative point of view, the macro-scale observations indicate the influence of the friction actuating on the external patch, whereas at the central patch where the bolt is fully tightened, there are no visible traces due to the frictional contact. Besides the three connections and contact patches on the interface, there are two holes of $\text{Ø}4$ mm that are dedicated for clamping purposes and one hole of $\text{Ø}5$ mm for the shaker/stinger attachment the testing beam. Details about the clamping procedure shall be mentioned herein.

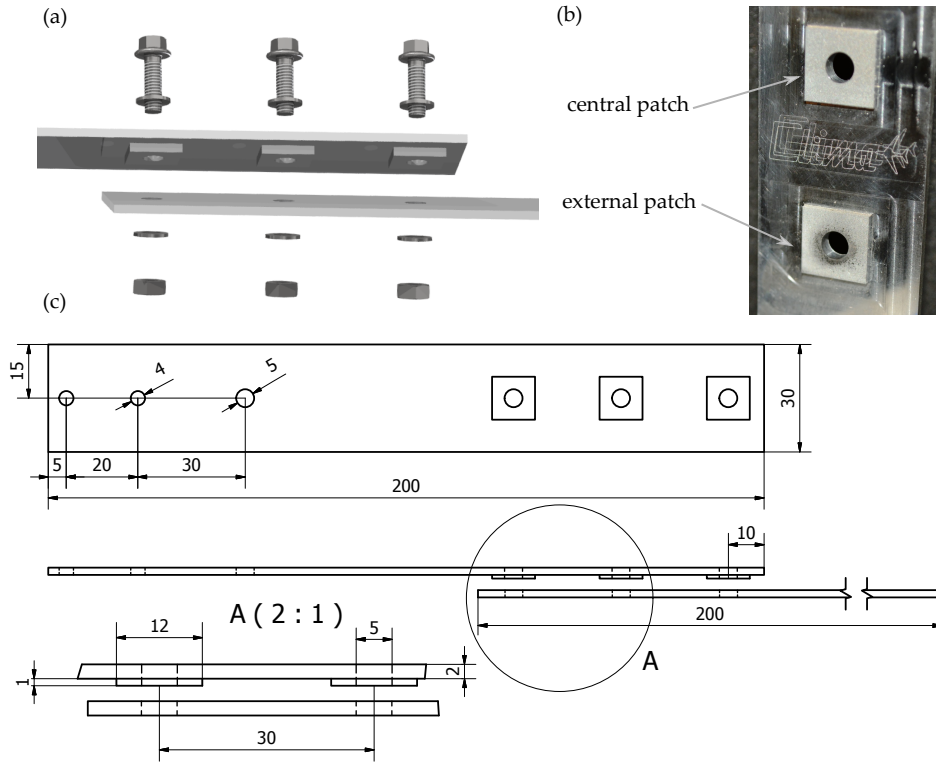


Figure 4: (a) Lap-joint 3D model CAD, which highlights the three contact patches, present only in one beam. (b) Patches beam picture. The central patch without friction marks because of the fully tightening, the external patch with friction marks because of the light tightening. (c) Lap-joint drawings CAD (lengths are in mm) - 2 beams, two clamp holes $\text{\O}4$ mm, one excitation hole $\text{\O}5$ mm, three contact patches.

2.2. Experimental setup

The experimental setup is shown in Fig. 5 consists of a lap-joint structure with dimensions of $370 \times 30 \times 2$ [mm], a load cell PCB 288D01, an electromagnetic Modal Shop shaker (Model K2004E01), a 3D scanning laser, NI9234 hardware for data acquisition. For all measurements, the beam with the contact patches is completely clamped on one side. Thus, to minimize uncertainties related to the stiffness in the boundary condition [21], a length of 30 mm is glued and screwed into a massive steel block. The excitation is performed by the shaker placed near the clamped end and placed on the beam's centerline to avoid exciting torsional modes and to reduce the shaker-structure interaction [22]. A threaded nylon rod stinger is used to transmit force in the stiff axial direction and reduce lateral loads to the experimental

235 test bench. To avoid the effect of gravity as well as the presence of torsional modes on vibrational behavior of the beam once bending modes are in interest, the structure is positioned vertically with its neutral line perpendicular to the ground.

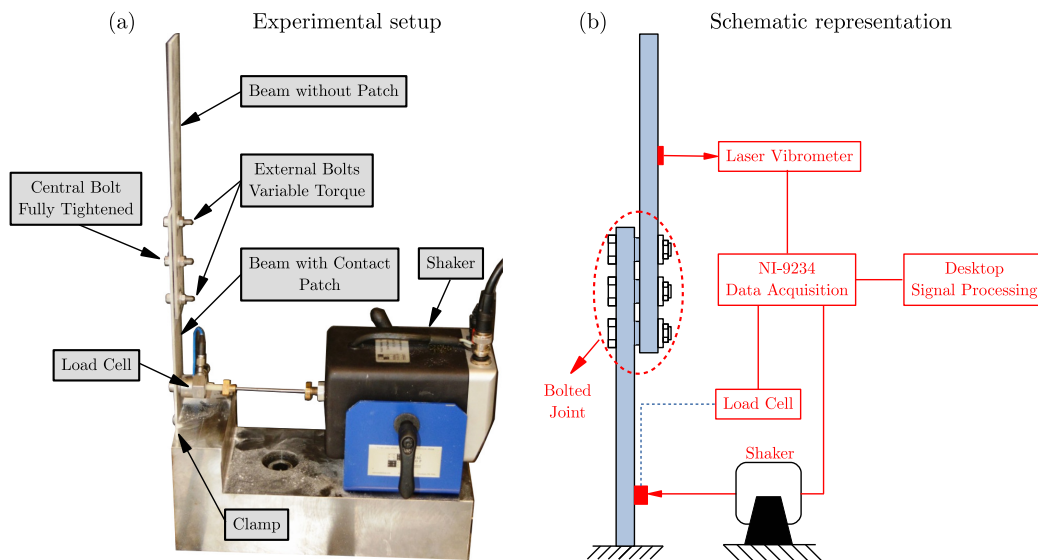


Figure 5: Experimental setup picture

240 For the assembly procedure, we follow the three-step protocol: firstly, to guarantee the alignment between both beams, two-axis are inserted in the external holes; then, the central bolt is fully tightened with a torque of 80 cNm; finally, both axes are removed, and the external bolts are thus tightened. The tightening torques applied on the external bolts are 10 cNm, 20 cNm, 30 cNm, and 80 cNm, to observe their influence on the structure's response. This screw ensures the stiffness of the assembly during the tests. 245 The tightening torque at the central bolt was checked after each experimental run using a Lindstorm MA500-1 torque wrench.

250 Before the experimental campaign started, the force applied from each tightening torque was measured with a Futek LTH300 donut load cell. Table 1 presents the associated force and the equivalent joint pressure of each torque condition and the coefficient of variation λ [%], defined as the standard deviation over the mean of the variable after several tests. The force ranges from 136 N (10 cNm) to 877 N (80 cNm), equivalent to contact pressures of 0.94 MPa and 6.09 MPa, respectively. These values correspond to

255 typical mean joint pressure values applied in practice (between 5 Pa and
 200 MPa) [23]. Although the maximum torque value considered is far from
 the upper limit used in practice, its value was satisfactory for the applica-
 tion investigated, concerning the excitation level considered. Further, note
 that the variation around low torque values is more notable, which highlight
 260 the complexities of dealing with jointed structures, once even the tightening
 torque carries uncertainties in its values.

| Torque [cNm] | Force [N] | Pressure [MPa] | λ [%] |
|--------------|-----------|----------------|---------------|
| 10 | 136.42 | 0.94 | 7.35 |
| 20 | 260.61 | 1.80 | 7.09 |
| 30 | 384.75 | 2.97 | 8.31 |
| 80 | 877.17 | 6.09 | 4.45 |

Table 1: Associated force and the equivalent joint pressure for each tightening torque applied and its coefficient of variation.

The choice of the torque values in Tab. 1 was supported by prelimi-
 nary studies involving the lap-joint in the glued condition (monolithic struc-
 ture). The variation in terms of stiffness and damping between the glued and
 265 80 cNm preload is not expressive, as shown in section 4. Thus, this value was
 set as the upper limit. In contrast, the 10, 20, and 30 cNm values applied
 to the contact patches indicate that there is a trade-off between increased
 damping and reduced joint pressure, without significant changes in stiffness.

2.3. *Vibration sensing*

270 The signal response has to be acquired in a less invasive manner to con-
 duct the experimental tests as well as possible. The accelerometers are ef-
 ficient as measuring instruments, but the wires may introduce uncertainties
 or errors in the measurements in terms of bias [24], especially for lightweight
 structures. A wireless accelerometer can be used to mitigate this problem,
 275 but the sensor mass may also induce uncertainties. In this context, the mea-
 surements are performed using the contactless Polytec vibrometer PSV-500
 with a 3D scanning laser. Its working distance is between 125 mm and 100 m.
 Its minimum resolution is 10 nanometers per second.

Two measurement types will be presented. Firstly, a complete laser scan-
 280 ning spans the whole structure through 195 sensing points distributed on
 the Orion beam surface. The scanning provides global structure behavior
 and allows obtaining experimental eigenvalues and eigenvectors. Then, to

highlight the nonlinear behavior of the structure according to the excitation amplitude as well as to evaluate the influences of the tightening torque, only one measurement point is kept positioned at a distance of 30 mm from the upper external patch center, which makes it easier to conduct a more significant number of measurements involving several torque conditions and excitation amplitudes, thus reducing the elapsed time between experimental tests. Figure 5(b) illustrates a schematic representation of the experimental apparatus.

3. EXCITATION DESIGN

As mentioned in the introduction, several excitation types are commonly used to study the dynamic behavior. The impact test is widespread and practical for measuring frequency response functions. This kind of excitation is not subject to the mass and stiffness effects of the shaker attachment, and it is helpful for linear structures. The input power spectrum is broadband, and it can excite a wide frequency range [12, 25]. It is also an interesting type of excitation to infer information from the effect of components external to the testing structure related to boundary conditions and instrumentation, as investigated by Smith et al. (2015) [24] in a series of testing scenarios involving the BRB benchmark. However, exciting nonlinearities through impact testing is a difficult task. Nevertheless, recent works have explored the transient response for the nonlinear model updating of bolted jointed structures [26, 27].

Still, regarding excitation techniques useful for modal analysis, the random excitation signals have a fundamental role in their practical implementation of exciting the structure with varying amplitude and reaching a wide frequency range. However, when considering this excitation type for identifying nonlinear systems and depending on the nonlinearity severity, the nonlinear effects in the system's output may be mistaken for noise disturbances. This may be a limitation of random excitations in dealing with nonlinear systems [28, 29].

One of the main advantages of using controlled periodic excitations lies in selecting a frequency range. It is possible to characterize, locate, and quantify the nonlinear distortions on the system's response. Sweeping sine tests provide an attractive, cost-effective ratio between the magnitude of excitation level and testing time [30]. However, as clarified by Dion et al. (2013) [14, 17], for weakly damped natural modes, the sweep rate shall be appropriately chosen to avoid modulations between natural frequencies and exci-

320 tation ones. Special attention must also be given to step-sine, and stop-sine
 tests, commonly used for mode isolation through force appropriation meth-
 ods, jump-up and jump-down testing to characterize nonlinearities, harmonic
 component analysis, among other applications [22, 31, 19]. When compared
 with sweeping sine tests, both step and stop-sine may require a long testing
 325 time.

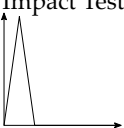
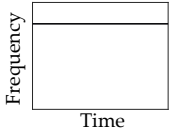
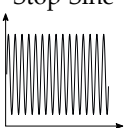
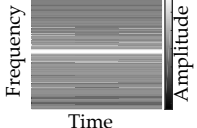
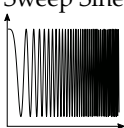
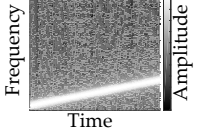
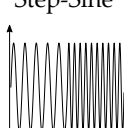
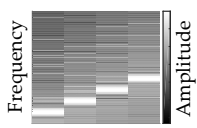

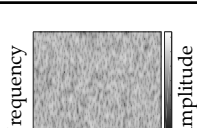
| Input | Time-Frequency | Benefits | Disadvantages |
|--|---|--|---|
| Impact Test  |  | <ul style="list-style-type: none"> • Practical and fast testing; • Broadband excitation. | <ul style="list-style-type: none"> • Difficult to excite nonlinearities. |
| Stop-Sine  |  | <ul style="list-style-type: none"> • Single frequency excitation; • Highlight harmonics in system response. | <ul style="list-style-type: none"> • Narrow-banded spectrum. |
| Sweep Sine  |  | <ul style="list-style-type: none"> • Adjustable frequency band; • Adjustable sweep rate. | <ul style="list-style-type: none"> • Modulations between resonant frequencies and excitation ones. |
| Step-Sine  |  | <ul style="list-style-type: none"> • Adjustable frequency band; • Jump-up and jump-down testing; • Steady-state response. | <ul style="list-style-type: none"> • Long time testing; • Amplitude control. |
| Random  |  | <ul style="list-style-type: none"> • Broadband excitation; • Linear modal testing. | <ul style="list-style-type: none"> • Difficult to excite nonlinearities. |

Figure 6: Comparison between different excitation types.

Figure 6 presents a compilation of the excitation strategies here discussed, as well as a comparison between each excitation in the time-frequency domain. Of course, several variants exist for each excitation technique, for instance, burst-random, multi-sine, and other. However, the main idea behind this section is to present, among several excitation types, which one may provide the most accurate excitation in the context of our study. Further
 330

discussion on this subject is found in [32, 33].

335 A shaker conducted the excitation of the structure placed 30 mm from
the clamped end of the Orion beam (Fig. 5) to minimize the shaker-structure
interaction. Initially, for preliminary tests with the global scan of the assem-
bled structure, a frequency-controlled white noise between 10 Hz and 2000 Hz
with low excitation amplitude was applied. It is essential to point out that,
at this excitation condition, the structure's underlying linear model can be
estimated.

340 There is an effort in the literature to propose experimental practices for
dynamic analysis and development of predictive dynamic models related to
excitation design. Ewins et al. (2015) [34] introduced a modal testing frame-
work for validating structural models that is useful when establishing ex-
perimental test procedures involving nonlinear analysis. The primary task of
345 identifying a nonlinear feature is subdivided into the detection of early signals
of nonlinearity, characterization of the physical origins of nonlinear effects,
location of the source of nonlinearity, and quantification of the strength of
nonlinearity. It is emphasized that the sequence in which these steps are
presented need not necessarily be followed if there is a fundamental under-
350 standing of the dynamic system under analysis.

Extending this framework to the implementation of experimental tests on
the Orion beam, the lap-joint of the structure is the source of the nonlinear
behavior. Once the aspects of the location of nonlinearities have been dis-
cussed, the next step is to detect which vibrating modes present early signs
355 of nonlinear features. Then, the best alternative to characterize how the
tightening of the external bolts influences the dry friction effects on the sys-
tem's response is conducting step-sine tests around resonant frequencies to
isolate nonlinear modes. Once that features involving friction and microslip
behavior exhibit a degree of amplitude dependence, the structure is subject
360 to several excitation amplitudes to quantify nonlinearity strength. In this
regard, one of the main problems faced by step-sine tests is the difficulty in
controlling the amplitude of the excitation force, especially in the vicinity
of the resonances due to the force drop off phenomenon [35]. One way to
observe this if a load cell is not available to inspect the force response is
365 through the presence of saw tooth effects in peak amplitudes of frequency
curves.

There are possibilities to reduce/eliminate limitations in the amplitude
control of the applied force. Shaker amplifiers can operate in current mode,
in which the output voltage is adjusted to maintain the required current at

370 the amplifier output. In this scenario, the force generated by the shaker is constant (proportional to the current supplied) but divided into two parts: one part excites the shaker itself, and the other excites the structure. As a consequence, the force applied to the beam is dependent on the dynamic stiffness of the shaker and the dynamic stiffness of the structure [36]. Thus, 375 to overcome these limitations and achieve a constant excitation amplitude as the frequency changes, the root means square (RMS) values of the applied force measured directly by the load cell were controlled using a real-time feedback controller. Figure 7 depicts the block diagram of the controller designed, whereas Appendix B brings forward the script algorithm executed.

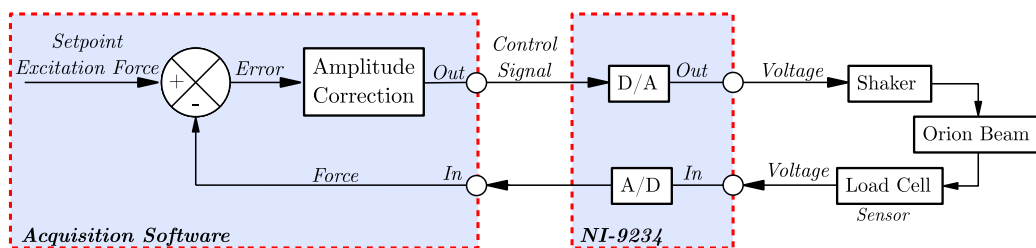


Figure 7: Block diagram of the feedback controller of the excitation force. The current excitation force is compared to the desired one (setpoint), and the error is calculated. Then, the controller evaluates at which position of the control law it is must actuate. The voltage control signal is converted and applied to the shaker, which excites the Orion beam. The load cell measures the force applied and feeds back their values to be compared to the setpoint once again, and the process is restarted. For more details regarding the algorithm script, see Appendix B

380 Figure 8 exemplifies the need for considering the amplitude control during step-sine tests. In this case, a low amplitude level of 10 mN is desired around the frequency ranging from 1700 to 1775 Hz. Note that the supplied voltage in the shaker amplifier from Fig. 8(a) reaches peak values around the vicinity of resonance (see Fig. 10) to keep a constant force amplitude, as illustrated in Fig. 8(b). Still, in Fig. 8(b), the excitation amplitude lies within the maximum acceptable error, with values around 9.8 mN and 10.2 mN. Finally, Fig. 8(c) illustrates the iterations until convergence for each frequency increment. The real-time controller presents more iterations for the first excitation frequency, in which the user sets the initial voltage amplitude and in the vicinity of the resonance frequency. The proposed controller exhibits satisfactory performance for the conditions examined in this 390

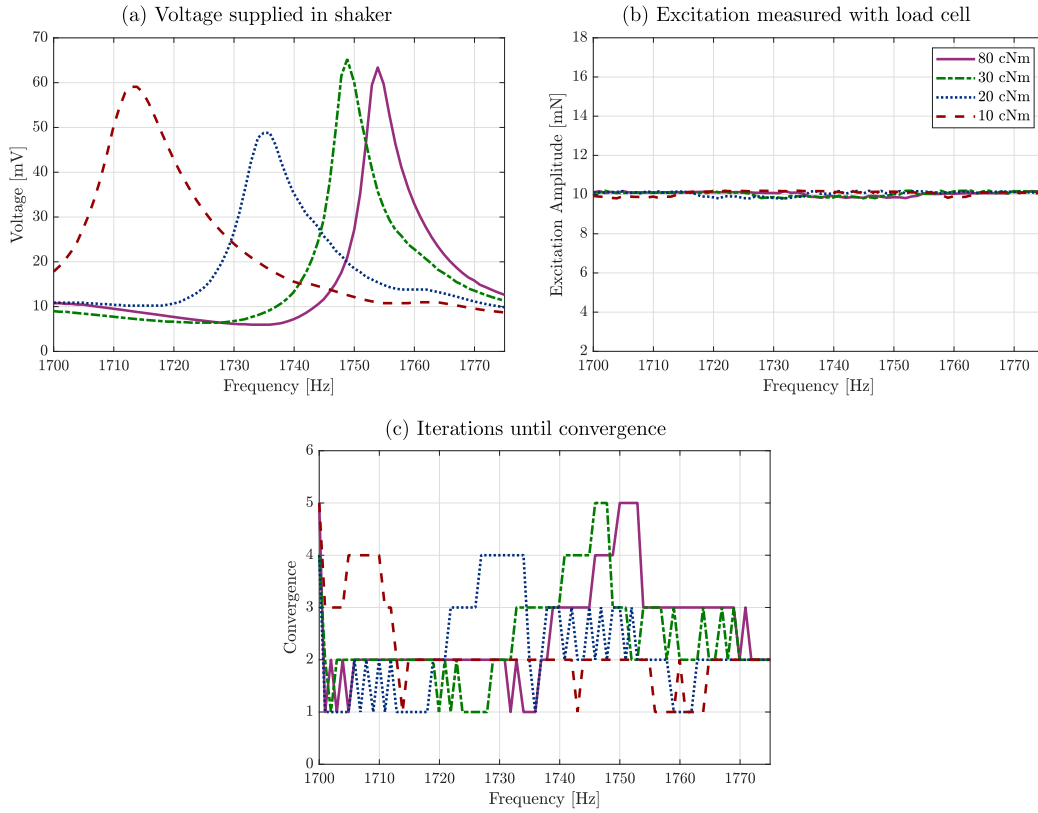


Figure 8: Representative example of the real-time controller actuating on the excitation amplitude.

work, providing the amplitude control with a small number of iterations. Likewise, the control strategy presents limitations related to supplying high voltage values in the shaker amplifier for conditions where it drives the control to its upper bound. To avoid problems related to the voltage supply required to maintain the force constant, Catalfamo et al. (2016) [37] investigated the acceleration amplitude control in the BRB, taking measurements close to the shaker driving point. The advantage in considering acceleration as a reference in a control strategy lies in the fact that resonance regions promote higher acceleration amplitudes to the whole structure, thus requiring lower current supply to the shaker. It is stressed that the algorithm presented in Appendix B can also be redefined to control another physical variable of interest, such as using acceleration measurements close to the driving point.

The controlled RMS force values were 10, 50, 100, 150, 200, and 250 mN,

405 whereas the maximum excitation amplitude was selected to keep the structural integrity. The shaker's voltages are distant from its maximum acceptable input voltage range for reaching these forcing values.

4. EXPERIMENTAL RESULTS

This section presents the Orion beam's primary results, starting with the white noise excitation, followed by the discussion on the measurements' repeatability. The influence of the tightening torque on the system's response, the impact of the excitation amplitude on the structure's nonlinear behavior, and finally, the frequency response curves predicted by the Duffing-Van der Pol oscillator are presented in direct comparison with experimental measurements. 415

4.1. Underlying linear structure

Figure 9(a) presents the frequency response function of the Orion beam considering the patches perfectly glued, which represents the monolithic state, and estimated after applying a low-amplitude white noise excitation (63.45 mN RMS) band-limited between 10 Hz and 2000 Hz. Six bending modes, corresponding to the first 19.38 Hz, second 122.5 Hz, third 289.38 Hz, fourth 723.8 Hz, fifth 922.5 Hz and sixth 1758 Hz modes were identified in the FRF data. The measurements indicate a low mode coupling (light modal density) in the frequency range around the 1st, 2nd, 3rd and 6th modes. Note the presence of the first torsional mode (546.30 Hz) between the third and fourth bending modes, but even so, its response amplitude is lower than the other modes shown in the FRF. The 4th and 5th modes are relatively close, in a frequency range with considerable modal density due to the presence also of torsional effects on the 5th vibrating mode, which is probably caused by effects of undesired moments at the driving point during the random excitation. 420 425 430

Figure 9(b) exemplifies the modes predicted experimentally considering 195 sensing points on the Orion beam's surface. Note that the energy delivered by the white noise excitation around the first bending mode was not enough to visualize the beam vibrating uniformly. The visualization of the fifth mode, in turn, presents a contribution of the torsional mode. Nevertheless, the displacement around the clamped end is nearly zero for all modes, confirming the clamping procedure's effectiveness. 435

The third and sixth bending modes present modal shapes that promote a pronounced deformation around the lap joint. Due to this reason, these 440

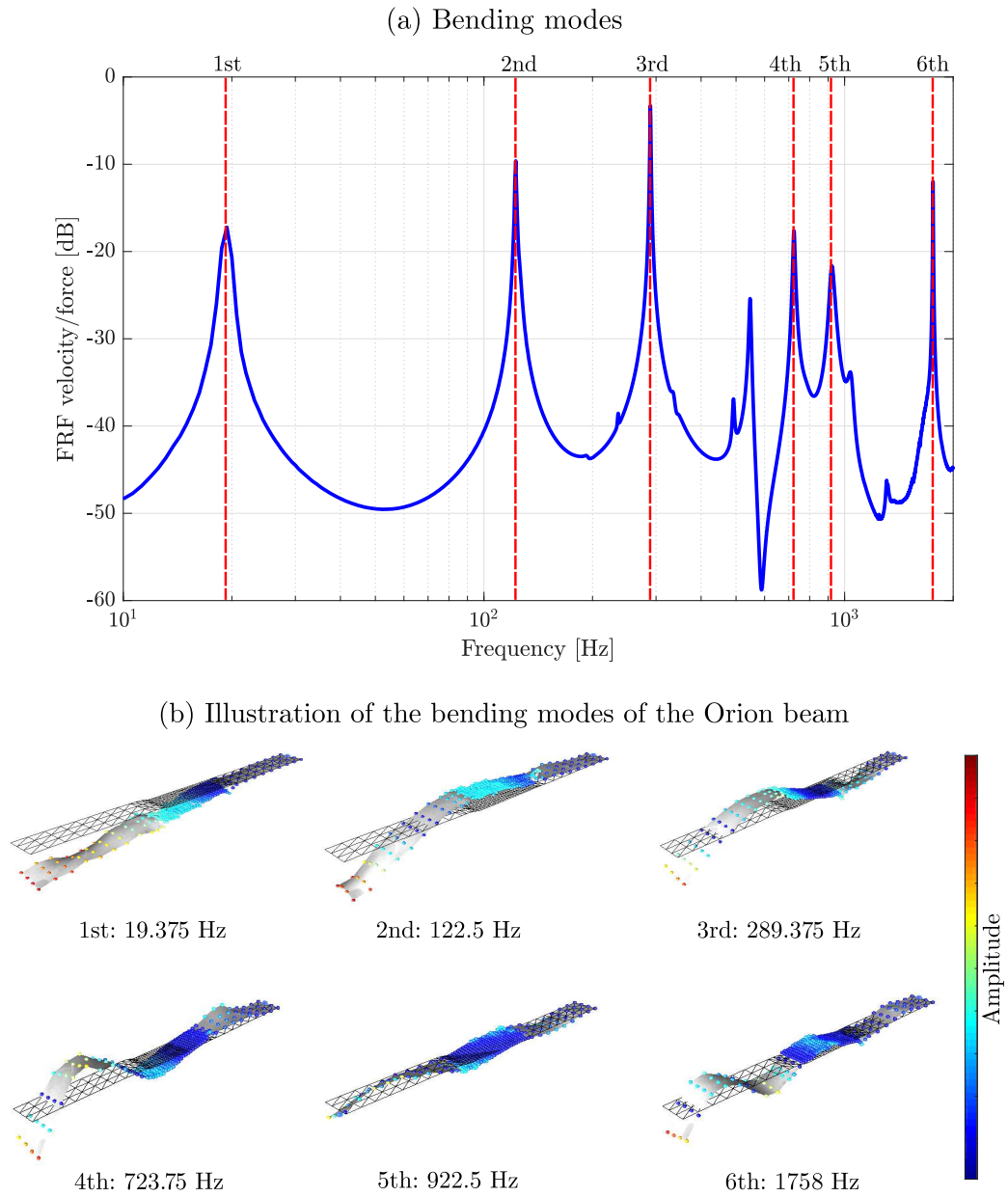


Figure 9: FRF velocity from the experimental result.

modes were potential candidates to investigate the nonlinear behavior induced by friction effects as well as the contribution of the tightening torque in the system's response. A preliminary analysis based on the step-sine tests

is conducted to highlight the amplitude-dependent effect.

445 The following section starts by presenting the third vibration mode and then focuses on the frequency response curves around the sixth bending mode considering several tightening torques and excitation amplitudes, as after preliminary analysis considering harmonic excitations, it was found that the latter mode is the most affected by nonlinearity.

450 4.2. On the Orion beam's response

All the frequency curves presented subsequently correspond to the one-point measurement (see Fig. 5), which provides proper observability on the bending modes of interest. The excitation force is feedback controlled following the block diagram previously presented in Fig. 7. The following
455 parameters are defined: step-sine with a time 5.12 seconds in steady-state motion at each step; and a sampling frequency of 25.6 kHz.

Moreover, three representative quantities are investigated: the resonance frequency f_n [Hz], the peak amplitude of the frequency response curves A_{\max} [dB] and the half-power bandwidth at -3dB Δ_{BW} [Hz]. These parameters indirectly estimate the evolution of the structure's damping and stiffness,
460 providing the necessary understanding of Orion benchmark behavior when subjected to the external variables of excitation level and tightening torque.

4.2.1. On the third vibrating mode's response

The preliminary frequency response curves related to the 3rd mode are
465 illustrated in Fig. 10 by considering two tightening torque conditions, 20 and 80 cNm, and several excitation amplitudes, 10 mN to 200 mN. In those curves, step-sine tests are starting at 280 Hz up to 300 Hz with a frequency increment of 0.3901 Hz. It is worth noting that for this vibrating mode, the central bolt is located close to the nodal point, and thus, the influence of
470 external bolts is enhanced.

For low excitation amplitudes, the resonance frequencies for both torque conditions, i.e., 289.1 Hz for 80 cNm and 287.9 for 20 cNm, are close to the resonance visualized for the glued condition during tests with random excitation. Although the softening effects can be visualized under these preloads as
475 the excitation amplitude increases, the special feature of the frequency curves is the amplitude attenuation. Figure 11 presents the shift in f_n , A_{\max} and -3 dB Δ_{BW} parameters. In Fig. 11(b), for a torque condition of 80 cNm, note that the peak amplitudes vary from -1.1 dB to -10.24 dB as the excitation increases, representing an absolute amplitude attenuation of 89%, whereas

480 for 20 cNm, there is a similar trend from -2.55 dB to -10.39 dB, but with an
attenuation of 75%. The increase of the -3 dB Δ_{BW} bandwidth related to
the excitation amplitude, as illustrated in Fig. 3 for both torque conditions,
highlights the influence of the frictional effects on the structural damping
485 significantly changing the nominal frequency of the structure, as seen in Fig.
11(a).

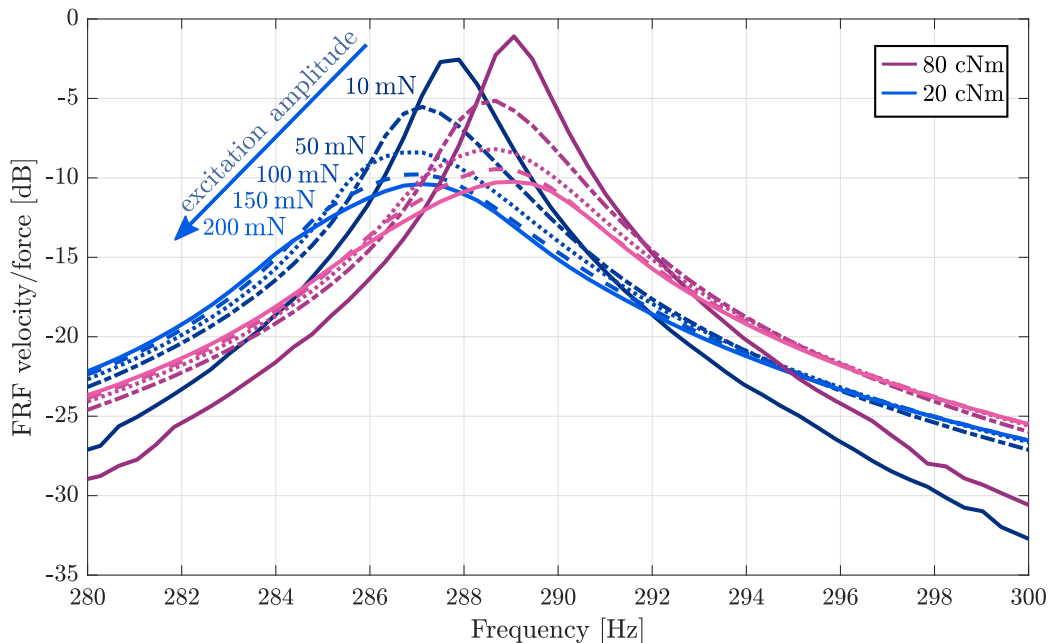


Figure 10: Nonlinear behavior of the Orion lap-joint around 280 and 300 Hz for different torques (80 cNm and 20 cNm) distinguished by different colors, and for multiple excitation level (10 mN to 200 mN) distinguished by different line types and gradient color.

The investigations conducted in this section are only to introduce a preliminary analysis of the Orion beam’s behavior and highlight the different roles played by the bolts in the structure’s response. The frequency changes
490 are pretty small since the central patch is close to a nodal point, and the energy dissipation can be mainly attributed to the external patches. The advantage of dealing with the other mode compared to the one presented in this section is in the possibility of subjecting the three contact patches to similar displacements, which also highlights nonlinear effects related to
495 softening stiffness. This paper’s following sections present a detailed dis-

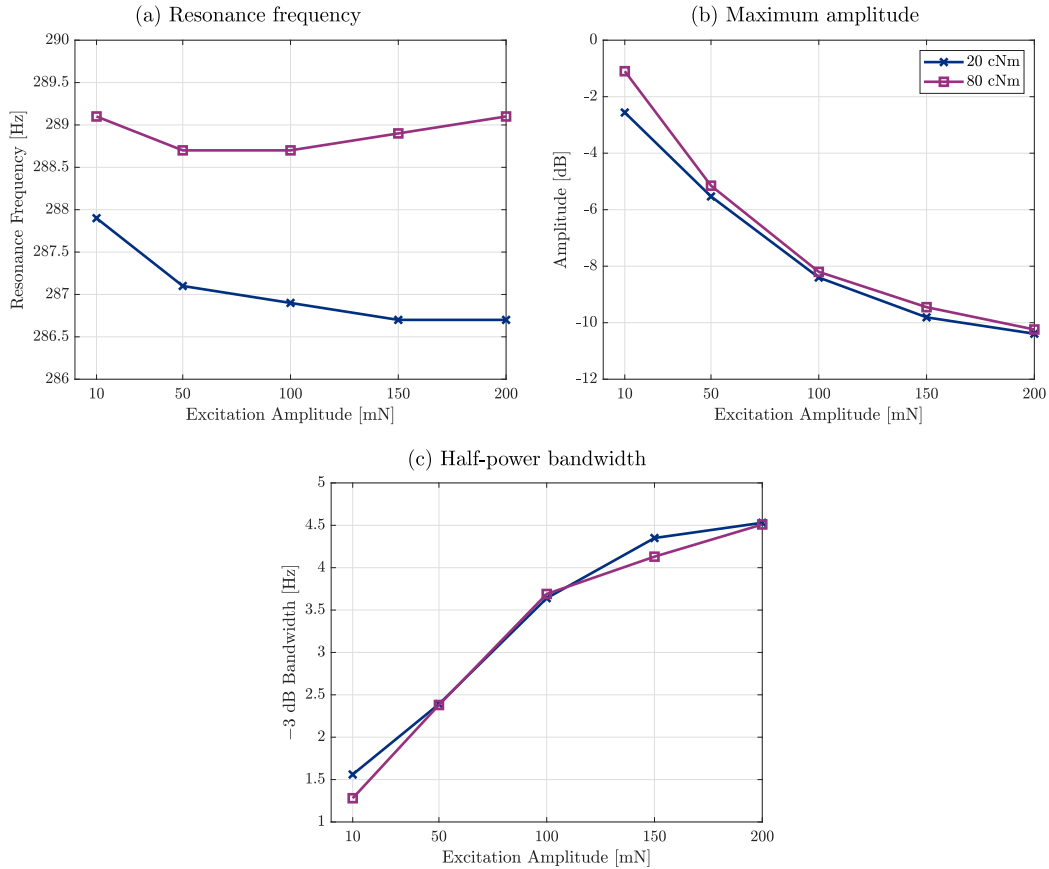


Figure 11: Nonlinear behavior of the Orion lap-joint around 280 and 300 Hz for different torques (80 cNm and 20 cNm) distinguished by different colors, and for multiple excitation level (10 mN to 200 mN) distinguished by different line types and gradient color.

cussion on the 6th bending mode from different perspectives outlined after experimental tests.

4.2.2. Measurements repeatability

This subsection aims to provide the degree of uncertainties of the results by studying the stability of the assembly and the repeatability of the measurements. This section tries to respond to the question: “How much can we trust the experimental measurements?” With the ambition, people could use these data to validate their numerical models.

The Orion beam is built with thin components and has the contact interface concentrated at each patch. Thus, due to the small area at each bolt,

the lap-joint connection occurs only under the pressure cone [38]. Recently, Brake et al. (2019) [39] presented an extensive study about the variability and repeatability of the BRB benchmark considering several modifications on the interface of the beams. One of the profiles investigated has small contact pads at the lap joint, similar to the Orion beam design. Although the conditions observed by the authors are related to the linear behavior, the repeatability of the small pad system is significantly higher than the nominal BRB design [12]. Recent research results, including [39], have indicated that reducing the contact area to the pressure cones should reduce the uncertainty in the structure response once the frictional dissipation is more negligible [40, 41].

In this context, to verify whether the Orion beam ensures repeatability among several experimental measurements, two sides are then studied: the tightening/loosening of the bolts in different orders and the complete tightening of the upper beam (the one without patches, see Fig. 5). Then, based on several assemblies and disassemblies of the lap-joint, the mean values μ , standard deviation σ , and coefficient of variation λ [%], are estimated. Besides, unlike the analysis presented by Brake et al. (2019) [39], the repeatability analysis through this subsection addresses nonlinearities in the structure behavior.

Figure 12 presents the frequency response curve of the structure considering a tightening torque of 80 cNm and two excitation amplitudes of 10 mN (low-level) and 250 mN (high-level) controlled by the feedback algorithm. All step-sine tests conducted for the mode of interest start at 1660 Hz up to 1780 Hz with a frequency increment of 1 Hz. The data variation represented by the figure appears due to seven experimental realizations. Furthermore, after each run, the lap-joint is completely disassembled and then reassembled. Table 2 summarizes the obtained results for the testing conditions. Note that, at the excitation amplitude of 10 mN, λ values for the parameters f_n , A_{\max} and Δ_{BW} are higher than the ones obtained at 250 mN. This may be explained by the fact that the energy delivered for high excitation levels is higher than the low amplitudes, minimizing uncertainties related to the measurement procedure. Additionally, for both excitation amplitudes, the variation λ of the parameters A_{\max} and Δ_{BW} presents higher values than the f_n variation, which is associated mainly to the stiffness of the jointed structure. The structure exhibits considerable repeatability at 80 cNm, even considering a high excitation amplitude. As investigated by Dossogne et al. (2017) [41], these results are expected for designs that have small contact

545 areas, like the Orion beam, since the uncertainties on the contact pressure are reduced, and the torque of 80 cNm leads to a significant preload.

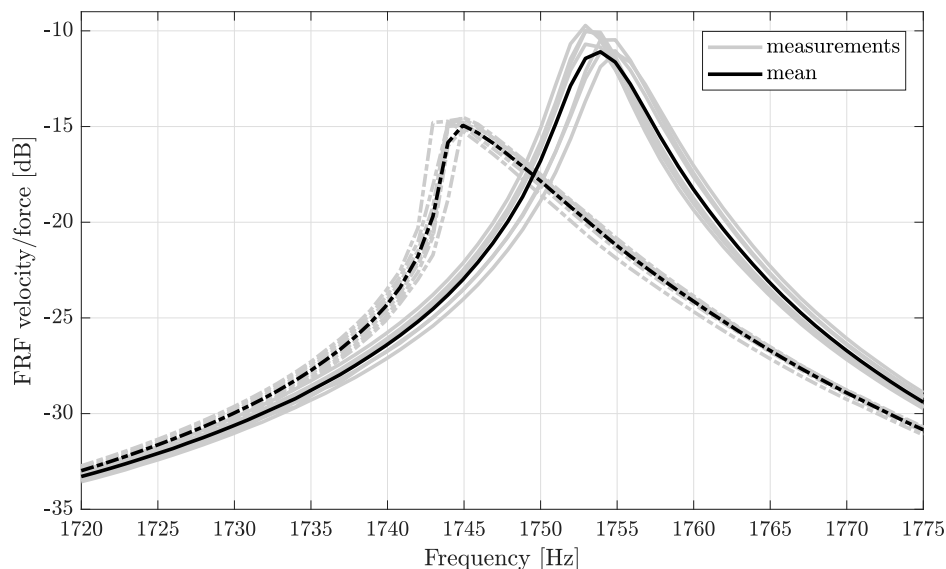


Figure 12: Repeatability of the measurements for seven experimental runs in frequency response curves considering a tightening torques of 80 cNm and excitation amplitudes of 10 mN (solid line —) and 250 mN (dash line - -); — represents the mean value for 7 lap-joint disassemblies, see Table 2.

| | 10 mN | | | 250 mN | | |
|----------------------|------------|----------|---------------|------------|----------|---------------|
| 80 cNm | μ | σ | λ [%] | μ | σ | λ [%] |
| f_n | 1753.71 Hz | 0.86 Hz | 0.05 | 1744.55 Hz | 0.51 Hz | 0.03 |
| A_{\max} | -10.45 dB | 0.55 dB | 5.26 | -14.80 dB | 0.22 dB | 1.48 |
| Δ_{BW} | 4.76 Hz | 0.32 Hz | 6.72 | 6.59 Hz | 0.30 Hz | 4.55 |

Table 2: Repeatability of the measurements for seven experimental runs with disassembly of the lap-joint and considering a tightening torque of 80 Nm at two excitation amplitudes of 10 mN (low-level) and 250 mN (high-level). Mean values (μ), standard deviations (σ) and coefficients of variation (CV) of the parameters f_n , A_{\max} and Δ_{BW} , see Fig. 12.

To investigate the variability induced by changes in the tightening torque, Fig. 13 presents several measurements considering a tightening torque of 20 cNm and the low level of excitation amplitude 10 mN. Figure 13(a) presents the frequency response curves of four experimental runs after com-

550 plete disassembly, whereas Fig. 13(b) also depicts four experimental real-
 izations, but considering tightening/loosening of the bolts. The changes be-
 tween the testing conditions are evident: all the coefficients of variance on the
 structure with disassembly are higher than the ones without disassembly, es-
 pecially for the parameters A_{\max} and Δ_{BW} . These results indicate that when
 555 the tightening torque assumes lower values, even with the structure operat-
 ing linearly, the reassembly process significantly changes the patches' contact
 surface profile. This process consequently increases the variability of the sys-
 tem's responses. Additionally, a direct comparison between the tightening
 torques of 20 cNm and 80 cNm, both at low excitation level, shows that
 560 the λ values of f_n , A_{\max} and Δ_{BW} for 20 cNm are higher than the ones for
 80 cNm. The low excitation amplitude allows observing only the impact of
 the tightening torque in the structure's response. Considering this, Table 1
 provides an intuitive justification of why that happens once the variations
 around low torque values (10, 20, and 30 cNm) are more significant than for
 565 the highest preload (80 cNm).

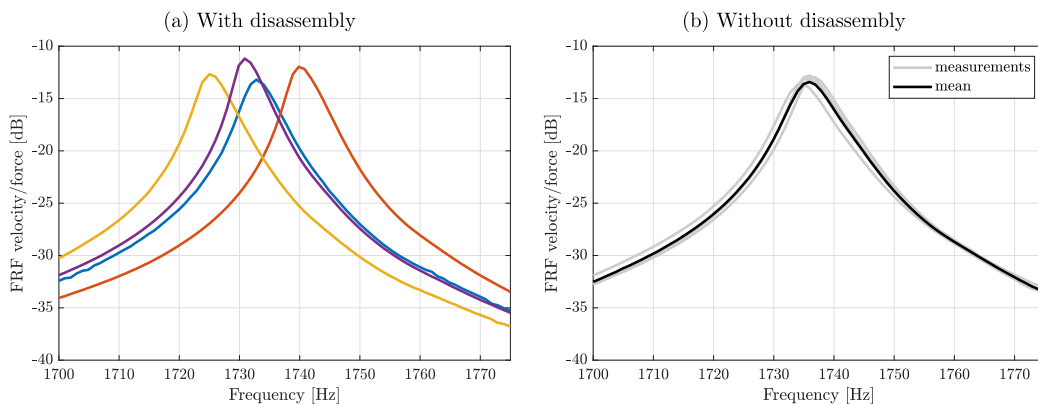


Figure 13: Repeatability of the measurements in frequency response curves considering a tightening torque of 20 cNm and low excitation amplitude 10 mN. Figure 13(a) represents the measurements with the complete disassembly of the lap-joint (solid-lines), whereas Fig. 13(b) depicts the measurements without the disassembly, but with tightening/loosening of the bolts (—), see Table 3.

| 20 cNm | With disassembly | | | Without disassembly | | |
|----------------------|-------------------------|----------|---------------|----------------------------|----------|---------------|
| | μ | σ | λ [%] | μ | σ | λ [%] |
| f_n | 1732.16 Hz | 6.11 Hz | 0.35 | 1735.66 Hz | 0.91 Hz | 0.05 |
| A_{\max} | -12.26 dB | 0.87 dB | 7.09 | -13.10 dB | 0.36 dB | 2.75 |
| Δ_{BW} | 6.17 Hz | 0.61 Hz | 9.88 | 7.83 Hz | 0.43 Hz | 5.49 |

Table 3: Repeatability of the measurements considering a tightening torque of 20 cNm and an excitation level of 10 mN. Mean values (μ), standard deviations (σ) and coefficients of variation (CV) of the parameters f_n , A_{\max} and Δ_{BW} ; for four measurements with the disassembly of the lap-joint and 4 measurements without the disassembly, but considering tightening/loosening of the bolts in different orders, see Fig. 13

As pointed by Ewins (2016) [42], joints are a source of epistemic uncertainty in structural dynamics, with emphasis on the fact that the order of tightening bolts can yield different static configuration to the system. From the modeling point of view, predicting these deviations could become a potential issue. Testing runs without complete disassembly may be proposed to mitigate this problem. Figure 13(b) shows that the loosening/tightening of the bolts and the order in which the bolts are tightened have almost no impact on the dynamic behavior.

On the one hand, another opportunity is to measure the tightening torque at the bolt during the experimental campaign, just employing strain gauges at the screw head. Measuring this parameter may be desirable to detect mechanisms for frictional energy dissipation within a connected surface, and be helpful in reducing epistemic uncertainty as direct measurements on contact mechanics become available. On the other hand, the patches' functions' reliability, i. e., the static and damping functions are based on the pressure distribution on interfaces considering various tightening conditions. This analysis, together with information about the tightening torque in experimental campaigns, will provide not only more extraordinary insight into the appearance of black traces on external patches, as seen in Fig. 4(b), but also how repeatability relates to interactions on the contact surface of the Orion beam.

4.2.3. On the influence of the tightening torque

Tests were conducted at a low excitation amplitude (10 mN) to highlight only the tightening torque's influence on the Orion benchmark. The frequency response curves considering several preload conditions are depicted in Fig. 14. Two characteristics stand out in this figure: the decrease in the

resonance frequency when the tightening torque also decreases, showing that the lap-joint inevitably softens the total rigidity of the system; a greater attenuation of the vibration amplitude for lower tightening values, indicating that the damping patches lead to greater energy dissipation. Table 4 evaluates the impact of the tightening torque on the parameters f_n , A_{\max} , Δ_{BW} . The results in Table 4 also indicate that there exists a similar trend between the frequency attenuation band Δ_{BW} and the tightening torque since energy dissipation processes also influence this parameter. The frequency response curves considering several preload conditions are depicted in Fig. 14. Two characteristics stand out in this figure: the decrease in the resonance frequency when the tightening torque also decreases, showing that the lap-joint inevitably softens the total rigidity of the system; a greater attenuation of the vibration amplitude for lower tightening values, indicating that the damping patches lead to greater energy dissipation. Table 4 evaluates the impact of the tightening torque on the parameters f_n , A_{\max} , Δ_{BW} . The results in Table 4 also indicate that there exists a similar trend between the frequency attenuation band Δ_{BW} and the tightening torque since energy dissipation processes also influence this parameter.

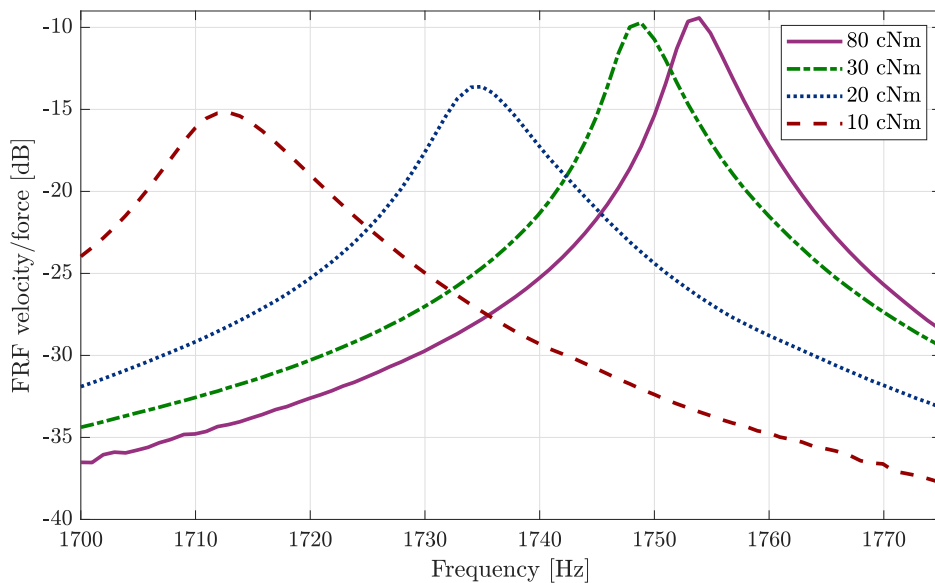


Figure 14: Torque impact at 10 mN excitation level.

The peak amplitudes vary from -9.40 dB for 80 cNm to -14.30 dB for 10 cNm, representing an absolute amplitude attenuation of 52%. The res-

onance frequency also changes, from 1754 Hz for 80 cNm, to 1714 Hz for 10 cNm. However, the frequency changes are small (2.28 %) compared with variations in amplitude. This feature indicates that, even for conditions
615 where the structure presents a behavior without early signs of nonlinearity in the frequency response curve, it is possible to attenuate vibration amplitudes without significantly compromising the structure’s stiffness just by controlling the contact in the patches. Although the recent work developed for the BRB benchmark [39] discusses the influence of several design param-
620 eters, including modifications on the contact surface, roughness tests, among others, the contribution sought by the Orion beam is new and ponders about the possibility of exploring the benefits that a lap-joint may offer for damping purposes without compromising the structural integrity.

| Torque [cNm] | f_n [Hz] | A_{\max} [dB] | Δ_{BW} [Hz] |
|--------------|------------|-----------------|---------------------------|
| 10 | 1714 | -14.28 | 9.90 |
| 20 | 1735 | -13.62 | 8.43 |
| 30 | 1749 | -9.71 | 5.18 |
| 80 | 1754 | -9.43 | 4.97 |

Table 4: Torque impact at 10 mN excitation level.

4.2.4. On the influence of the excitation amplitudes

625 After tests involving the influence of the tightening torque on the structure’s behavior, this section aims to assess the impact of the nonlinear effects on the Orion beam’s response when subjected to different excitation amplitudes.

Figure 15 shows the frequency response curves in terms of amplitude (Fig. 15(a)) and phase (Fig. 15(b)) of the Orion beam considering six excitation levels at the tightening torque of 10 cNm. As several lap-joint benchmarks, the Orion beam presents amplitude-dependent nonlinearities. One of the most prominent characteristics in the frequency *versus* amplitude plot is the resonant frequency decreasing as the excitation level increases, e.g., decreasing from 1713 Hz to 1695 Hz for the excitation amplitudes of 10 and 250 mN,
635 respectively. This so-called softening effect occurs, especially in jointed structures, due to the partial slippage on the joint interface, which reduces the contact stiffness [4, 11]. Moreover, it should also be stressed that peak amplitudes have a clear trend of reducing their values when the excitation level
640 increases, which indicates the amplitude-dependence of the damping on the

structure displacement. For the frequency increment of 1 Hz, the Orion beam does not present jump-up frequencies in step-sine tests. Additionally, even for high excitation levels, the frequency response curves do not exhibit the dropout effect around the resonant frequencies, which shows the effectiveness of the feedback controller applied.

Figure 16 summarizes the Orion lap joints nonlinear behavior around the sixth bending mode according to excitation levels and torques. The softening effect is present in all assembly conditions. Although the glued state also shows variations in the resonance frequency, the structure's behavior is only moderately altered. The frequency decreases by 3 Hz from low to high excitation amplitudes, representing a variation of 0.17%. In this condition, the joint pressure is high, and the linearity assumption sufficiently represents the system's behavior. For a torque level of 80 cNm and excitation force at 10 mN, the changes in frequency and peak amplitudes concerning the glued condition are not expressive, a shift of 4 Hz in frequency and an absolute difference between peaks of 0.21 dB, respectively. One can see that torque values above 80 cNm could have been selected, but there would be no substantial changes regarding resonant frequencies at low excitation amplitudes.

Furthermore, through these frequency response curves that combine several conditions, one of the main issues involving modeling lap-joints arises. There is a superposition between the response curves, which is difficult for modeling differences if a law to describe the tightening torque is not taken into account. Studies that consider a multi-scale analysis to capture the evolution of the frictional effects over time and frequency are still developed [43].

To clarify how excitation and torque contribute to each frequency response, Fig. 17 depicts the variations on the parameters f_n , A_{\max} , Δ_{BW} . The Orion beam allows distinguishing properly how the external variables influence the analyzed parameters. For instance, Fig. 17 (a) shows the evolution of the resonance frequency versus excitation amplitude considering several tightening torques. In this figure: the observed values of resonance frequencies are slightly higher as the tightening torque increases; the frequency shift from low (10 mN) to high (250 mN) excitation amplitudes has more prominent values for low preload (10 cNm) with an absolute difference of 19 Hz, whereas for high torque values the variation is 9 Hz.

Figure 17(c) depicts the evolution of the Δ_{BW} parameter. The -3 dB bandwidth is an estimator that works well in the case of damping, i.e., for linear systems. Nevertheless, it is a popular indicator for people who study

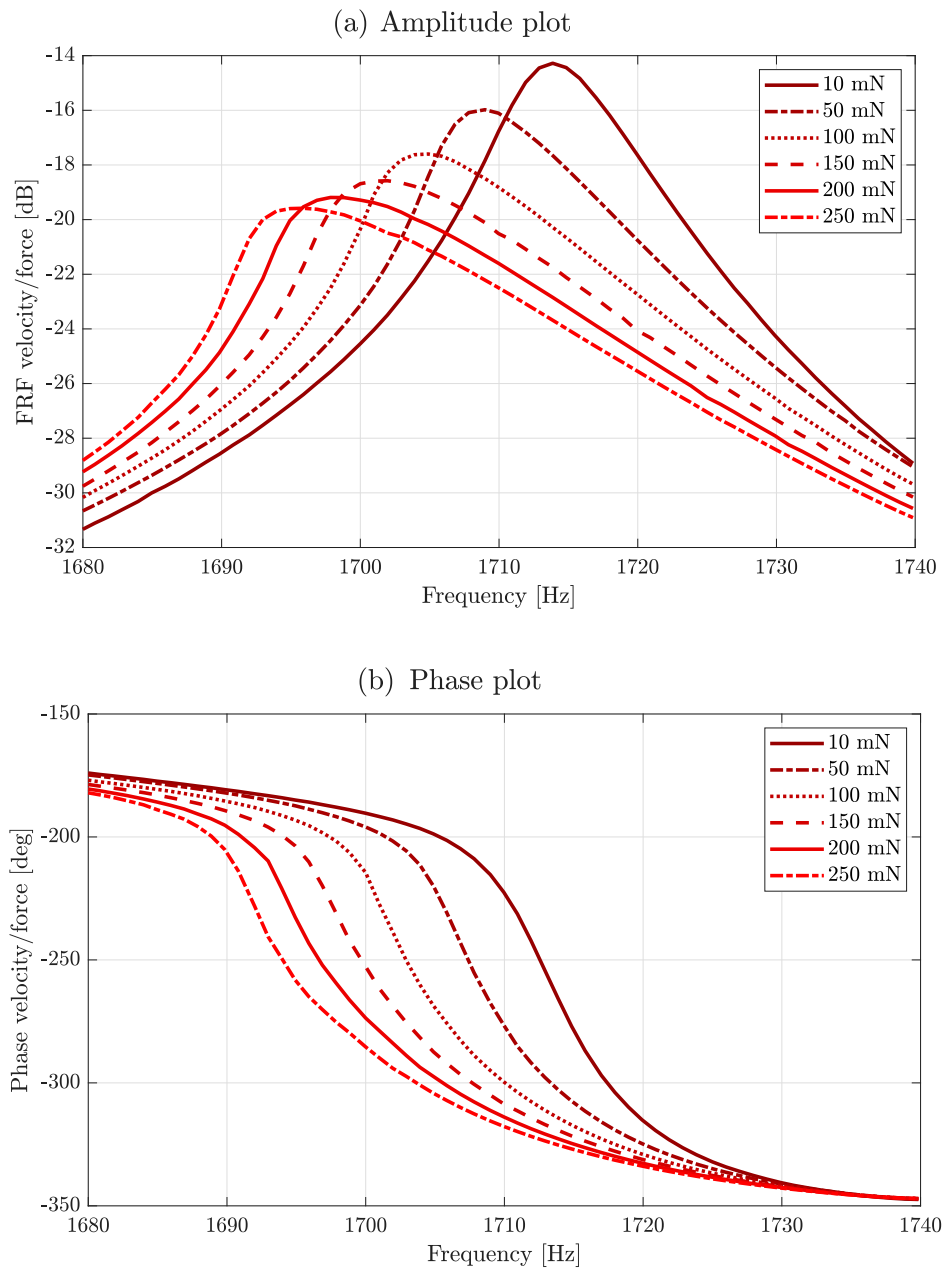


Figure 15: Excitation level impact at 10 cNm torque.

vibrations, but one has to be careful about its means.

680

In the investigations carried out in this work, two mechanisms cause the

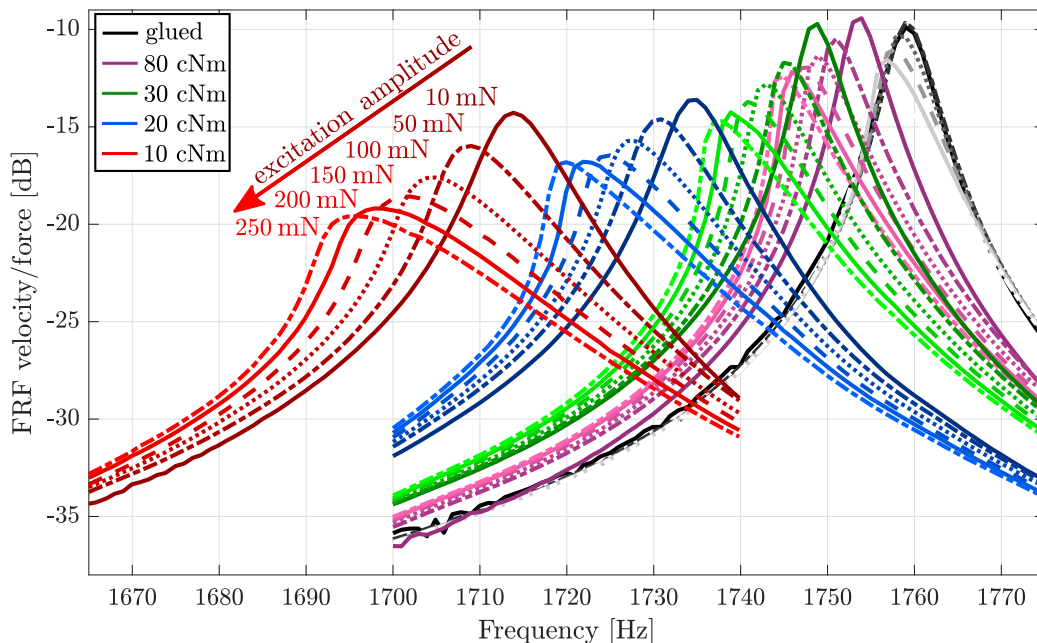


Figure 16: Nonlinear behavior of the Orion lap-joint around 1665 and 1775 Hz for different torques (80 cNm, 30 cNm, 20 cNm, and 10 cNm) distinguished by different colors, and for multiple excitation level (10 mN to 250 mN) distinguished by different line types and gradient color. The greyscale curves show the behavior of a glued assembly.

bandwidth to evolve: energy dissipation by friction and structure softening. Frictional energy dissipation leads to an asymptotic evolution of the vibration attenuation when full slip occurs. However, this condition was never reached during testing. The loss of stiffness acts as a softening nonlinearity. It leads to the peak being laid down on the left and the bandwidth being widened if the damping is sufficient. If the damping is not sufficient concerning the softening effect, the bandwidth no longer increases and may even decrease. This is what happens with 20, 30, 80 cNm tightening torques above the 200 mN amplitude. When both increase simultaneously, the bandwidth increases continuously. This is the case for the 10 cNm torque. Moreover, the estimation of the half-power bandwidth is sensitive to the frequency increment adopted during the step-sine tests. Thus, since the A_{\max} parameter is the reference for computing the half-power bandwidth, its results may show minor discrepancies.

Table 5 presents a comparison between the relative variations that the parameters of resonance frequency and amplitude attenuation undergo be-

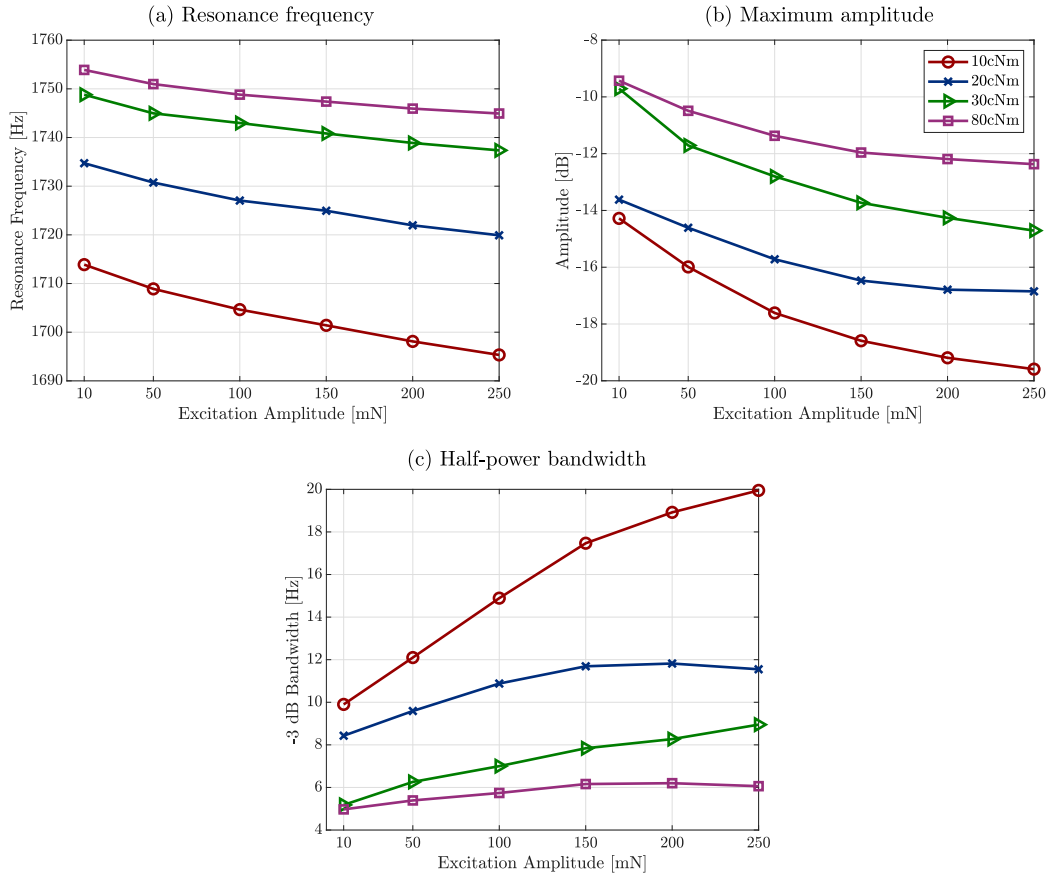


Figure 17: Analysis of the Orion beam around 1665 and 1775 Hz. Torque and level impact on (a) the natural frequency, (b) the maximum amplitude and (c) the half-power bandwidth.

tween the condition of the lowest excitation amplitude (10 mN) to the highest (250 mN). The variations in the response amplitude are relatively more significant than the variations observed in the resonance frequency. As expected, the friction effects on the Orion beam are more pronounced in amplitude attenuation than in stiffness changes.

This beam is intended to be an academic benchmark for the joints community, in which the frictional effects promoted by contact patches are used to improve damping. It is supposed that, when considering higher joint pressures and consequently reduction of microslip behavior, the response of the structure would be close to the behavior exhibited by the glued condi-

| Torque [cNm] | $ \Delta f_n $ [%] | $ \Delta A_{\max} $ [%] |
|--------------|--------------------|-------------------------|
| 10 | 1.1 | 31.18 |
| 20 | 0.86 | 51.49 |
| 30 | 0.68 | 23.72 |
| 80 | 0.50 | 38 |

Table 5: Variations of Δf_n and ΔA_{\max} in absolute values.

tion. However, the Orion beam paves the way for what could be explored in jointed structures in terms of taking advantage of the damping intrinsic to these systems without compromising stiffness in applications where amplitude attenuation is of utmost importance, for instance, designing optimization of bolted structures to act as tuned vibration dampers with dry friction damping.

4.3. Evaluation of the Duffing-Van der Pol oscillator for describing Orion beam's response

This section investigates the feasibility of proposing an SDoF model to describe the single-point measurements discussed above around the 6th bending mode of the Orion beam. Based on the nonlinear amplitude-dependent characteristics observed experimentally in the structure's response, an analytical Duffing-Van der Pol oscillator is considered [44]. It is argued that the presence of terms related to both nonlinear damping and nonlinear stiffness can describe the effects of amplitude attenuation and decrease resonance frequencies due to multiple levels of excitation.

The SDoF Duffing-Van der Pol oscillator is given by:

$$m\ddot{q}(t) + c\dot{q}(t) + kq(t) + \underbrace{\beta\dot{q}(t)q(t)^2}_{\text{nonlinear damping}} + \underbrace{\alpha q(t)^3}_{\text{nonlinear stiffness}} = F(t) \quad (1)$$

where m [kg], c [Ns/m] and k [N/m] are the equivalent mass, damping and stiffness coefficients, respectively, whereas β [Ns/m³] and α [N/m³] are coefficients responsible to project the nonlinear restoring forces on physical basis. Additionally, it is important to point out that the model is not used to directly describe the frictional forces in contact interfaces, but rather the generalized restoring forces that actuate the mode of interest.

Keeping in mind that steady-state measurements were acquired after step-sine tests applied in the resonance frequencies' vicinity, an identification technique is proposed. The methodology is developed into a harmonic

balance framework considering a first-order harmonic as a solution, once that the fundamental harmonic component at the excitation frequency is the most prominent, providing a way to capture the main characteristics present in the frequency response curves from Fig. 16. The main idea is to identify a unique set of SDoF Duffing-Van der Pol parameters for each tightening torque condition to track the evolution of the equivalent stiffness and damping and thus furnishing a better physical insight into the influence of tightening torque on the system's behavior over a wide range of excitations amplitude. Appendix C provides a complete description of the methodology developed for this work.

Table 6 presents the set of parameters calibrated considering the methodology described in Appendix C for the glued condition, whereas Fig. 18 shows the evolution of calibrated parameters as function of several tightening torque conditions. To emphasize the variations of m , c , k , α , and β when the preload varies, the identified values of glued condition (Table 6) are considered a reference and then used as normalization scale for other conditions.

| m [kg] | c [Ns/m] | $k \times 10^7$ [N/m] | $\beta \times 10^{11}$ [Ns/m ³] | $\alpha \times 10^{15}$ [N/m ³] |
|----------|------------|-----------------------|---|---|
| 0.0917 | 2.7946 | 1.1204 | 1.4862 | -2.0090 |

Table 6: Model parameters considering the glued condition for all excitation amplitudes.

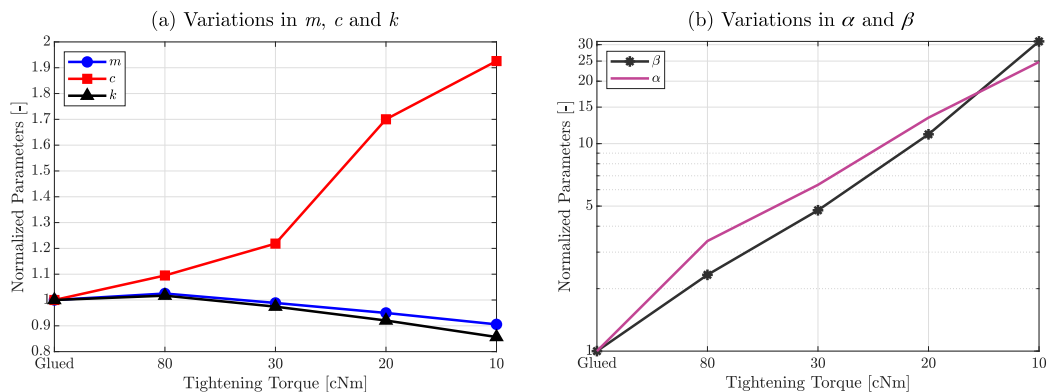


Figure 18: Evolution of calibrated parameters as function of several tightening torque conditions.

Based on the estimated parameters, some indicators can be stressed out. On the one hand, note that the equivalent coefficients of mass and stiffness

are decreasing as a function of the tightening torque in Fig. 18(a). The
750 formulation employed in equation (1) is equivalent to the representation of
uncoupled reduced-order models, which is usually considered to describe full
order Finite Element (FE) models but written on the physical basis [45].
Notwithstanding the foregoing, the equivalent comparison can also be pro-
posed: $m \equiv \Phi^T \mathbf{M} \Phi$ and $k \equiv \Phi^T \mathbf{K} \Phi$. Assuming the mass matrix constant,
755 whereas the modal mass changes according to the applied torque level, one
can note that the mode shapes change. The shape changes are small con-
sidering the numerical values and, therefore, validate assumptions made in
previous numerical works, which consider that contact nonlinearities alter
the mode shapes [11, 45]. Additionally, the experimental tests used to cal-
760 ibrate the model were performed consecutively without disassembly of the
setup. On the other hand, the equivalent damping coefficient almost doubled
its value from the glued condition to the preload of 10 cNm, detaching that
although m and k are sensitive to preload values changes, it is possible to
increase damping, preserving the structural stiffness.

765 Figure 18(b) depicts the evolution of β and α for different torque val-
ues. These parameters are the projection of nonlinear forces that actuate in
the 6th vibrating mode and show a significant increase in nonlinear terms'
contribution to the structure's behavior for tightening torques far from the
monolithic condition. Moreover, negative values of cubic stiffness α are ex-
770 pected once Fig. 16 indicates that the structure presents softening effects.

Figure 19 exhibits a comparison between the predicted frequency response
curves for several torque conditions *versus* the experimental ones for a excita-
tion level of 200 mN. Note that, despite its simplicity, the Duffing-Van der Pol
model proposed could reproduce with a satisfactory agreement with the ex-
775 perimental measurements. Table 7 presents the Duffing-Van der Pol model's
evaluation through the normalized mean square error (NMSE) between the
predicted responses and the experimental measurements for different torque
conditions and multiple excitation levels. Note that the model could repro-
duce better the measurements for the conditions glued and 80 cNm, since
780 for high preload values, the structure behavior is moderately altered by the
presence of nonlinear effects. Despite the differences between the model and
experimental measurements, the results have demonstrated that the excita-
tion design could uncouple the bending mode, allowing the SDoF nonlinear
model to reproduce the dynamics of the Orion beam present in the frequency
785 response curves properly. Additionally, the identification strategy has proven
to operate well, assuming the available experimental data from a single-point

measurement.

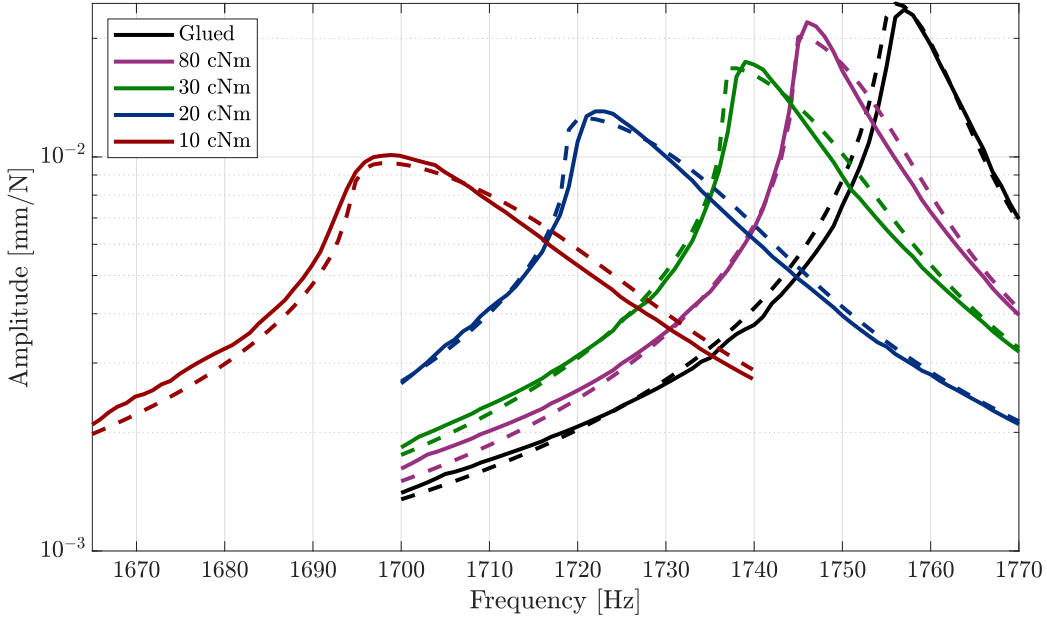


Figure 19: Comparison between the frequency response curves predicted by the Duffing-Van der Pol model (dashed lines — —) *versus* experimental measurements (solid lines —) for different torques (Glued, 80 cNm, 30 cNm, 20 cNm and 10 cNm) considering an excitation amplitude of 200 mN.

Several works propose to approximate isolated nonlinear modes of bolted structures based on SDoF models, such as those presented by Eriten et al. (2013) [46] and Segalman et al. (2015) [47]. A convenient discussion raised in both papers is that a single parametric model resulting from a specific data condition will not be globally descriptive. In parallel to this work, the same occurs with the Duffing-Van der Pol model proposed since, for each torque condition, a set of parameters had to be estimated. A limitation of the model that needs further investigation is its ability to predict the response for force values beyond 250 mN for low torque values such as 10 cNm, 20 cNm, and 30 cNm, since other effects are linked to micro-scale dynamics of the contact patches may be underestimated. Due to the polynomial form of the nonlinearity present in the proposed oscillator, it is also concluded that it would not be a satisfactory approximation for situations in which the structure undergoes macro slip, an effect that non-smooth models can characterize [48].

| NMSE [%] | 10 cNm | 20 cNm | 30 cNm | 80 cNm | Glued |
|----------|--------|--------|--------|--------|-------|
| 10 mN | 6.79 | 6.34 | 6.01 | 5.38 | 5.09 |
| 50 mN | 6.68 | 6.42 | 6.16 | 5.41 | 4.96 |
| 100 mN | 6.66 | 6.37 | 6.05 | 5.26 | 4.63 |
| 150 mN | 6.65 | 6.07 | 5.80 | 5.00 | 4.16 |
| 200 mN | 6.53 | 5.73 | 5.44 | 4.67 | 3.80 |
| 250 mN | 6.39 | 5.62 | 5.09 | 4.50 | 3.72 |

Table 7: Normalized mean square error between analytical responses and experimental data for several tightening torque conditions and multiple excitation level.

5. FINAL REMARKS

This work presented an overview of good practices for designing and ex-
805 perimenting with dynamically excited jointed structures, aiming to provide
more vibration damping without compromising structural integrity. All these
aspects were addressed considering the Orion beam, a new lap-joint configu-
ration with small contact patches at each bolt connection. The central bolt
is responsible for maintaining the nominal frequency by setting the normal
810 load with the fully tightening torque condition, whereas the external bolts
experience several tightening torques to assess how the friction effects affect
the system’s damping.

The experimental setup considered the clamped-free boundary condition
and a shaker attached close to the Orion beam’s clamped end. Step-sine
815 tests were adopted to study the dynamic behavior of the assembled system.
The interface load showed higher nonlinear properties. A feedback controller
was designed to perform an amplitude control, thus avoiding the force drop-
off phenomenon in the resonance frequencies’ vicinity. Regarding the Orion
beam’s design, results from subsection 4.2.1 related to the 3rd bending mode
820 introduced the influence of contact patches on the dynamic behavior of the
structure. One could verify that the contribution of the central patch to the
system’s damping is of less importance when compared to the contribution
of the external ones.

Although there exist pronounced variabilities in the system’s response af-
825 ter complete assembly and disassembly procedures, the structure maintained
impressive repeatability after several experimental measurements without
complete disassembly (see subsection 4.2.2). Contact patches, which are
proper to retain the contact interface on a small area, minimized dynamic

clearances and provided a contact pressure slightly sensitive to shape imper-
830 fections.

The effects of amplitude attenuation proved to be quite sensitive to changes
in the tightening torque applied in the external bolts. The Orion beam pre-
sented a more significant attenuation of the vibration amplitude for lower
tightening values, as showed Fig. 14, even operating in the linear regime
835 of motion. The results show that it is possible to benefit amplitude atten-
uation without significant losses in the contact stiffness. Alternatively, this
feature paves the way for proposing new control techniques of the vibration
amplitude in jointed structures based on the applied bolt preload. However,
caution with this approach is advised since it has only be demonstrated on
840 the present system configuration.

In comparison to the results presented for the 3rd mode, it is noted for the
6th mode that besides substantial vibration amplitude attenuation, there is
also a variation in frequency related to the softening effect for higher excita-
tion amplitudes. Thus, from the frequency curves of both vibration modes,
845 the results suggest that more pronounced displacements in the vicinity of
the central patch may lead to microslip, but of less importance than external
patches when considering torque values of 10, 20 and 30 cNm.

Furthermore, although the nonlinear behavior of the curves presented in
Fig. 16 was expected, i.e., the presence of softening effects as the excita-
850 tion amplitude increases, the new lap-joint configuration separated well the
correlations between the parameters analyzed for several torques and exci-
tation amplitudes since there is no overlapping among different curves and
conditions, as illustrated in Fig. 17. Therefore, this new lap-joint and the
results obtained can serve as a reference for researchers who wish to develop
855 methods for predicting damping in joints.

A Duffing-Van der Pol oscillator was proposed to approximate the exper-
imental measurements analytically. Simultaneously, the model parameters
could provide physical insight into how different tightening torque affects the
Orion beam's behavior. The parameters were estimated into a harmonic bal-
860 ance identification framework, as described in Appendix C. The performance
of the model could be improved by considering more harmonic terms in the
solution proposed. However, the analytical responses predicted the primary
characteristics present in the frequency response curves for several tight-
ening torques and multiple excitations amplitude. The equivalent stiffness was
865 moderately altered for several preload, whereas the equivalent damping al-
most doubled its value from the glued condition to the low preload condition,

which occurs due to patches in the Orion beam design.

870 Finally, the whole experimental measurements presented in this work, including the geometry design data, are open access. We suggest using this design and experimental tools to characterize the friction dissipation through the damping patches, induced micro-sliding, roughness, and flatnesses on the joint interface, to facilitate new techniques to measure and predict the nonlinear behavior of jointed structures.

ACKNOWLEDGMENTS

875 This works was supported by Bourgogne Franche-Comté Region in collaboration with EUR EIPHI Graduate School (contract ANR-17-EURE-0002). The authors are thankful for the “Fond Interministeriel Unique” that financially supports the project CLIMA, the “Bourse-Oréal UNESCO Pour les Femmes et la Science” that encourage women to make sciences, 880 and the financial support provided by the São Paulo Research Foundation (FAPESP/Brazil), grant numbers 2016/21973-5, 2019/06540-3 and 2019/19684-3 and the Brazilian National Council for Scientific and Technological Development (CNPq/Brazil), grant number 306526/2019-0.

APPENDIX A








| Pictogram | Signification |
|---|---|
|  | The normal load can be set without changing the nominal frequency |
|  | The joint is almost symmetric |
|  | The contact pressure is slightly sensitive to shape imperfections |
|  | The contact pressure is highly sensitive to shape imperfections |
|  | The normal load is sensitive to vibrations |
|  | Dynamic clearance may occur |
|  | Negation to previous propositions |

Table 8: List of pictograms and their meanings.

885 APPENDIX B

This Appendix introduces the script algorithm executed by the feedback controller from Fig. 7 for performing the feedback control and integrating software and measurement hardware. Although the algorithm was used for amplitude control of the excitation force, other kinematic quantities can be considered, such as acceleration measurements.

The algorithm is stated as follows:

1. the algorithm starts by defining the following parameters: increment and frequency range, desired excitation amplitude, the initial supply voltage of the shaker, the time duration of the test and sampling frequency;

2. the acquisition board converts the control signal, which is the voltage for supplying the exciter, from digital to analog. It then sends it to the shaker that contains an amplifier. During the vibrational testing, the load cell or the accelerometer measures the signal that corresponds to the applied force/acceleration by the shaker. Now, reversely, the acquisition hardware converts the output signal of the sensor and sends the measured voltage to the acquisition software;
3. the software converts the measured voltage to force or displacement and estimates its RMS value. The error ε between the experimental RMS \hat{F} [N] and the desired one F [N] is calculated:

$$\varepsilon = \frac{|\hat{F} - F|}{F} \quad (1)$$

Then, based on the error, the new voltage amplitude A_N [V] used to supply the shaker is corrected according to the voltage value A_{N-1} [V] from the last iteration following the simple controller design:

Algorithm 1: Amplitude correction.

Define convergence criteria: $(\varepsilon_{\max}, N_{\max})$;

if $1 - \frac{\varepsilon}{1.5} \leq 0$ **then**

$A_N = 0.1A_{N-1}$;

else if $1 - \frac{\varepsilon}{1.5} \geq 0$ **then**

$A_N = 2A_{N-1}$;

if $N > N_{\max}$ **then**

break;

end;

$u(t) = A_N \cos(\omega_i t)$;

where ε_{\max} denotes the maximum acceptable error and N_{\max} is the stop criterion based on the number of iterations until reaching the convergence; $u(t)$ [V] is the control signal and ω_i corresponds to the i^{th} excitation frequency during the step-sine testing. For this work, $\varepsilon_{\max} = 2\%$ and $N_{\max} = 20$. This simple algorithm is inspired on the bang-bang logic, in which the control law has two control positions (just

- as the bang-bang scheme) restricted to lower or upper limits for actuating. Each position is defined based on the error, which determines the magnitude of the voltage that must be applied to the shaker. The controller at position $1 - \frac{\varepsilon}{1.5} \geq 0$ considers a case where the applied voltage signal is further away from the desired one, whereas the position $1 - \frac{\varepsilon}{1.5} \leq 0$ reduces that value considerably to rest exactly around the desired error;
4. the acquisition board reads the control signal and sends it to the shaker;
 5. the real-time controller returns to the second step and restarts the controlling system while the error between the experimental RMS amplitude and the desired one is greater than ε_{\max} ;
 6. the excitation frequency is increased. The voltage amplitude of the previous increment updates the value of the initial voltage supplied in the shaker.

APPENDIX C

This section introduces the harmonic balance method applied to equation (1) to identify the model parameters. Since the frequency response curves were obtained through step-sine tests, equation (1) yields:

$$m\ddot{q}(t) + c\dot{q}(t) + kq(t) + \beta\dot{q}(t)q(t)^2 + \alpha q(t)^3 = F_e \sin(\Omega t) \quad (1)$$

Thus, assuming a first-order harmonic solution considering the complex representation:

$$q(t) = j \underbrace{(\mathcal{Q} - \overline{\mathcal{Q}})}_{=q_s} \sin(\Omega t) + \underbrace{(\mathcal{Q} + \overline{\mathcal{Q}})}_{=q_c} \cos(\Omega t) \quad (2)$$

where q_s and q_c are the harmonic coefficients, \mathcal{Q} and $\overline{\mathcal{Q}}$ are the fundamental harmonic amplitude and its complex conjugate, respectively, measured at the frequency Ω . Substituting equation (2) into equation (1) and balancing the harmonic terms:

$$(-m\Omega^2 + k)q_s - c\Omega q_c - \frac{\beta\Omega}{4} (q_c^3 - q_c q_s^2) + \frac{3\alpha}{4} (q_s^3 + q_c^2 q_s) = F_e \quad (3)$$

$$(-m\Omega^2 + k)q_c + c\Omega q_s + \frac{\beta\Omega}{4} (q_s^3 - q_s q_c^2) + \frac{3\alpha}{4} (q_c^3 + q_s^2 q_c) = 0 \quad (4)$$

Given equations (3)-(4), the model parameters are estimated by:

$$\begin{Bmatrix} m \\ c \\ k \\ \beta \\ \alpha \end{Bmatrix} = \begin{bmatrix} -\Omega^2 q_s & -\Omega q_c & q_s & \frac{\Omega}{4} (q_c^3 - q_c q_s^2) & \frac{3}{4} (q_s^3 + q_c^2 q_s) \\ -\Omega^2 q_c & \Omega q_s & q_c & \frac{\Omega}{4} (q_s^3 - q_s q_c^2) & \frac{3}{4} (q_c^3 + q_s^2 q_c) \end{bmatrix}^+ \begin{Bmatrix} F_e \\ 0 \end{Bmatrix} \quad (5)$$

where $(\bullet)^+$ denotes the pseudo-inverse matrix, the parameters are estimated over each torque condition's excitation band frequency. It is worth mentioning the work of Jalali et al. (2007) [49], which identified a set of parameters used to describe a nonlinear jointed structure through the harmonic balance framework. However, different from the formulation proposed here, which identifies the whole set of parameters present in the model equation based on harmonic components, Jalali et al. (2007) considered the nonlinear restoring force's computation for each excitation frequency.

References

- [1] J. Noël, M. Schoukens, F-16 aircraft benchmark based on ground vibration test data, in: 2017 Workshop on Nonlinear System Identification Benchmarks, Brussels, Belgium, 2017, pp. 19 – 23 (April 24-26 2017).
- [2] M.-A. Beaudoin, K. Behdian, Analytical lump model for the nonlinear dynamic response of bolted flanges in aero-engines casings, *Mechanical Systems and Signal Processing* 115 (2019) 14 – 28 (2019). doi:<https://doi.org/10.1016/j.ymssp.2018.05.056>. URL <https://www.sciencedirect.com/science/article/pii/S0888327018303157>
- [3] D. J. Segalman, Modelling joint friction in structural dynamics, *Structural Control and Health Monitoring* 13 (1) (2006) 430–453 (2006). doi:<https://doi.org/10.1002/stc.119>.
- [4] D. J. Segalman, A modal approach to modeling spatially distributed vibration energy dissipation, Tech. Rep. SAND2010-4763, Sandia National Laboratories, Albuquerque, New Mexico and Livermore, California (2010).

- 960 [5] S. Bograd, P. Reuß, A. Schmidt, L. Gaul, M. Mayer, Modelling the dynamics of mechanical joints, *Mechanical Systems and Signal Processing* 25 (8) (2011) 2801–2826 (2011). doi:<https://doi.org/10.1016/j.ymssp.2011.01.010>. URL <https://www.sciencedirect.com/science/article/pii/S0888327011000203>
- 965 [6] M. R. Brake, *The Mechanics of Jointed Structures: Recent Research and Open Challenges for Developing Predictive Models for Structural Dynamics*, Springer, 2017 (2017). doi:<https://doi.org/10.1007/978-3-319-56818-8>.
- 970 [7] H. Ahmadian, H. Jalali, Generic element formulation for modelling bolted lap joints, *Mechanical Systems and Signal Processing* 21 (5) (2007) 2318–2334 (2007). doi:<https://doi.org/10.1016/j.ymssp.2006.10.006>. URL <https://www.sciencedirect.com/science/article/pii/S0888327006002263>
- 975 [8] H. Ahmadian, H. Jalali, Identification of bolted lap joints parameters in assembled structures, *Mechanical Systems and Signal Processing* 21 (2) (2007) 1041–1050 (2007). doi:<https://doi.org/10.1016/j.ymssp.2005.08.015>. URL <https://www.sciencedirect.com/science/article/pii/S0888327005001263>
- 980 [9] Y. Song, Simulation of dynamics of beam structures with bolted joints using adjusted Iwan beam elements, *Journal of Sound and Vibration* 273 (1-2) (2004) 249–276 (2004). doi:[https://doi.org/10.1016/S0022-460X\(03\)00499-1](https://doi.org/10.1016/S0022-460X(03)00499-1). URL <https://www.sciencedirect.com/science/article/pii/S0022460X03004991>
- 985 [10] H. Jalali, H. Haddad Khodaparast, H. Madinei, M. Friswell, Stochastic modelling and updating of a joint contact interface, *Mechanical Systems and Signal Processing* 129 (2019) 645 – 658 (2019). doi:<https://doi.org/10.1016/j.ymssp.2019.04.003>.
- 990 [11] H. Festjens, G. Chevallier, J.-l. Dion, A numerical tool for the design of assembled structures under dynamic loads, *Interna-*

- tional Journal of Mechanical Sciences 75 (2013) 170–177 (2013).
doi:<https://doi.org/10.1016/j.ijmecsci.2013.06.013>.
URL <https://www.sciencedirect.com/science/article/pii/S0020740313001860>
- 995
- [12] M. R. Brake, P. Reuß, D. J. Segalman, L. Gaul, Variability and repeatability of jointed structures with frictional interfaces, in: Dynamics of Coupled Structures, Volume 1, Springer, 2014, pp. 245–252 (2014).
doi:https://doi.org/10.1007/978-3-319-04501-6_23.
- 1000 [13] N. Peyret, J.-L. Dion, G. Chevallier, P. Argoul, Micro-slip induced damping in planar contact under constant and uniform normal stress, International Journal of Applied Mechanics 02 (2) (2010) 281–304 (2010).
doi:<https://doi.org/10.1142/S1758825110000597>.
- [14] J.-L. Dion, G. Chevallier, N. Peyret, Improvement of measurement techniques for damping induced by micro-sliding, Mechanical Systems and Signal Processing 34 (1) (2013) 106–115 (2013).
doi:<https://doi.org/10.1016/j.ymsp.2012.08.003>.
URL <https://www.sciencedirect.com/science/article/pii/S0888327012003093>
- 1005
- [15] A. Singh, M. Scapolan, Y. Saito, M. S. Allen, D. Roettgen, B. Pacini, R. J. Kuether, Experimental characterization of a new benchmark structure for prediction of damping nonlinearity, in: Nonlinear Dynamics, Volume 1, Springer International Publishing, 2019, pp. 57–78 (2019).
doi:https://doi.org/10.1007/978-3-319-74280-9_6.
- 1010
- [16] M. Scheel, T. Weigele, M. Krack, Challenging an experimental non-linear modal analysis method with a new strongly friction-damped structure, Journal of Sound and Vibration 485 (2020) 115580 (2020).
doi:<https://doi.org/10.1016/j.jsv.2020.115580>.
URL <http://www.sciencedirect.com/science/article/pii/S0022460X20304120>
- 1020
- [17] N. Peyret, J.-L. Dion, G. Chevallier, A framework for backbone experimental tracking: Piezoelectric actuators, stop-sine signal and Kalman filtering, Mechanical Systems and Signal Processing 78 (2016) 28–42 (2016). doi:<https://doi.org/10.1016/j.ymsp.2015.09.020>.

- 1025 URL <https://www.sciencedirect.com/science/article/pii/S088832701500415X>
- [18] L. Gaul, J. Lenz, Nonlinear dynamics of structures assembled by bolted joints, *Acta Mechanica* 125 (1) (1997) 169–181 (Mar 1997). doi:<https://doi.org/10.1007/BF01177306>.
- 1030 [19] M. Scheel, S. Peter, R. I. Leine, M. Krack, A phase resonance approach for modal testing of structures with nonlinear dissipation, *Journal of Sound and Vibration* 435 (2018) 56–73 (2018). doi:<https://doi.org/10.1016/j.jsv.2018.07.010>.
URL <https://www.sciencedirect.com/science/article/pii/S0022460X18304486>
- 1035 [20] H. Bouaziz, N. Peyret, M. S. Abbes, G. Chevallier, M. Haddar, Vibration reduction of an assembly by control of the tightening load, *International Journal of Applied Mechanics* 08 (06) (2016) 1650081 (2016). doi:<https://doi.org/10.1142/S1758825116500812>.
- 1040 [21] T. Ritto, R. Sampaio, R. Aguiar, Uncertain boundary condition Bayesian identification from experimental data: A case study on a cantilever beam, *Mechanical Systems and Signal Processing* 68 (2016) 176–188 (2016). doi:<https://doi.org/10.1016/j.ymsp.2015.08.010>.
URL <https://www.sciencedirect.com/science/article/pii/S0888327015003714>
- 1045 [22] M. Peeters, G. Kerschen, J.-C. Golinval, Modal testing of nonlinear vibrating structures based on nonlinear normal modes: Experimental demonstration, *Mechanical Systems and Signal Processing* 25 (4) (2011) 1227–1247 (2011). doi:<https://doi.org/10.1016/j.ymsp.2010.11.006>.
URL <https://www.sciencedirect.com/science/article/pii/S0888327010003821>
- 1050 [23] S. Bograd, A. Schmidt, L. Gaul, Joint damping prediction by thin-layer elements, in: *Proceedings of IMAC XXVI: A Conference and Exposition on Structural Dynamics*, Orlando, FL, 2008 (2008).
- 1055 [24] S. Smith, J. Bilbao-Ludena, S. Catalfamo, M. Brake, P. Reuß, C. Schwingshackl, The effects of boundary conditions, measurement

- techniques, and excitation type on measurements of the properties of mechanical joints, in: Nonlinear Dynamics, Volume 1: Proceedings of the 33rd IMAC, A Conference and Exposition on Structural Dynamics, 2015, Springer, 2015, p. 415 (2015). doi:https://doi.org/10.1007/978-3-319-15221-9_36.
- 1060
- [25] P. Avitabile, Modal space-in our own little world, *Experimental Techniques* 39 (1) (2015) 3–10 (2015). doi:<https://doi.org/10.1111/j.1747-1567.2012.00846.x>.
- 1065
- [26] R. M. Lacayo, M. S. Allen, Updating structural models containing nonlinear Iwan joints using quasi-static modal analysis, *Mechanical systems and signal processing* 118 (2019) 133–157 (2019). doi:<https://doi.org/10.1016/j.ymsp.2018.08.034>.
URL <https://www.sciencedirect.com/science/article/pii/S0888327018305739>
- 1070
- [27] P.-P. Yuan, W.-X. Ren, J. Zhang, Dynamic tests and model updating of nonlinear beam structures with bolted joints, *Mechanical Systems and Signal Processing* 126 (2019) 193–210 (2019). doi:<https://doi.org/10.1016/j.ymsp.2019.02.033>.
URL <https://www.sciencedirect.com/science/article/pii/S0888327019301141>
- 1075
- [28] T. Caughey, Response of a nonlinear string to random loading, *Journal of Applied Mechanics* 26 (3) (1959) 341–344 (1959).
- [29] J. Schoukens, L. Ljung, Nonlinear System Identification: A User-Oriented Road Map, *IEEE Control Systems Magazine* 39 (6) (2019) 28–99 (2019). doi:<https://doi.org/10.1109/MCS.2019.2938121>.
- 1080
- [30] G. Gloth, M. Sinapius, Analysis of swept-sine runs during modal identification, *Mechanical Systems and Signal Processing* 18 (6) (2004) 1421 – 1441 (2004). doi:[https://doi.org/10.1016/S0888-3270\(03\)00087-6](https://doi.org/10.1016/S0888-3270(03)00087-6).
URL <http://www.sciencedirect.com/science/article/pii/S0888327003000876>
- 1085
- [31] B. Tang, M. Brennan, J. V Lopes, S. da Silva, R. Ramlan, Using non-linear jumps to estimate cubic stiffness nonlinearity: An experimental
- 1090

- study, Proceedings of the Institution of Mechanical Engineers, Part C: Journal of Mechanical Engineering Science 230 (19) (2016) 3575–3581 (2016). doi:<https://doi.org/10.1177/0954406215606746>.
- 1095 [32] K. Worden, G. R. Tomlinson, Nonlinearity in structural dynamics: detection, identification and modelling, Institute of Physics Publishing, Bristol and Philadelphia, 2001 (2001).
- [33] D. J. Ewins, Modal testing: theory, practice and application, John Wiley & Sons, 2009 (2009).
- 1100 [34] D. J. Ewins, B. Weekes, A. delli Carri, Modal testing for model validation of structures with discrete nonlinearities, Philosophical Transactions of the Royal Society A: Mathematical, Physical and Engineering Sciences 373 (2051) (2015) 20140410 (Sep. 2015). doi:<https://doi.org/10.1098/rsta.2014.0410>.
- 1105 [35] M. A. Peres, R. W. Bono, D. L. Brown, Practical aspects of shaker measurements for modal testing, in: Proceedings of the ISMA, 2010, pp. 2539–2550 (2010).
- [36] B. Tang, M. Brennan, G. Gatti, Use of the dynamic stiffness method to interpret experimental data from a nonlinear system, Journal of Sound and Vibration 421 (2018) 91–110 (2018). doi:<https://doi.org/10.1016/j.jsv.2018.01.006>.
URL <https://www.sciencedirect.com/science/article/pii/S0022460X18300063>
- 1110 [37] S. Catalfamo, S. A. Smith, F. Morlock, M. R. Brake, P. Reuß, C. W. Schwingshackl, W. Zhu, Effects of experimental methods on the measurements of a nonlinear structure, in: Dynamics of Coupled Structures, Volume 4, Springer, 2016, pp. 491–500 (2016).
- 1115 [38] M. Masuko, Y. Ito, K. Yoshida, Theoretical analysis for a damping ratio of a jointed cantibeam, Bulletin of JSME 16 (99) (1973) 1421–1432 (1973). doi:<https://doi.org/10.1299/jsme1958.16.1421>.
- 1120 [39] M. Brake, C. Schwingshackl, P. Reuß, Observations of variability and repeatability in jointed structures, Mechanical Systems and Signal Processing 129 (2019) 282 – 307 (2019).

- doi:<https://doi.org/10.1016/j.ymsp.2019.04.020>.
URL <http://www.sciencedirect.com/science/article/pii/S0888327019302511>
- 1125
- [40] H. Goyder, P. Ind, D. Brown, Measurement of Damping due to Bolted Joints, in: ASME: International Design Engineering Technical Conferences and Computers and Information in Engineering Conference, 2013 (2013). doi:<https://doi.org/10.1115/DETC2013-12826>.
- 1130 [41] T. Dossogne, T. W. Jerome, D. P. T. Lancereau, S. A. Smith, M. R. W. Brake, B. R. Pacini, P. Reuß, C. W. Schwingshackl, Experimental assessment of the influence of interface geometries on structural dynamic response, in: Dynamics of Coupled Structures, Volume 4, Springer International Publishing, Cham, 2017, pp. 255–261 (2017). doi:https://doi.org/10.1007/978-3-319-54930-9_22.
- 1135
- [42] D. J. Ewins, Exciting vibrations: the role of testing in an era of supercomputers and uncertainties, *Meccanica* 51 (2016) 3241–3258 (2016). doi:<https://doi.org/10.1007/s11012-016-0576-y>.
- [43] N. N. Balaji, W. Chen, M. R. Brake, Traction-based multi-scale nonlinear dynamic modeling of bolted joints: Formulation, application, and trends in micro-scale interface evolution, *Mechanical Systems and Signal Processing* 139 (2020) 106615 (2020). doi:<https://doi.org/10.1016/j.ymsp.2020.106615>.
- 1140
- URL <http://www.sciencedirect.com/science/article/pii/S0888327020300017>
- 1145
- [44] S. Masri, J. Caffrey, T. Caughey, A. Smyth, A. Chassiakos, Identification of the state equation in complex non-linear systems, *International Journal of Non-Linear Mechanics* 39 (7) (2004) 1111 – 1127 (2004). doi:[https://doi.org/10.1016/S0020-7462\(03\)00109-4](https://doi.org/10.1016/S0020-7462(03)00109-4).
- 1150
- URL <http://www.sciencedirect.com/science/article/pii/S0020746203001094>
- [45] H. Festjens, G. Chevallier, J. Dion, Nonlinear model order reduction of jointed structures for dynamic analysis, *Journal of Sound and Vibration* 333 (7) (2014) 2100 – 2113 (2014). doi:<https://doi.org/10.1016/j.jsv.2013.11.039>.
- 1155

URL <http://www.sciencedirect.com/science/article/pii/S0022460X13009930>

- 1160 [46] M. Eriten, M. Kurt, G. Luo, D. Michael McFarland, L. A. Bergman, A. F. Vakakis, Nonlinear system identification of frictional effects in a beam with a bolted joint connection, *Mechanical Systems and Signal Processing* 39 (1) (2013) 245–264 (2013). doi:<https://doi.org/10.1016/j.ymssp.2013.03.003>.
URL <https://www.sciencedirect.com/science/article/pii/S0888327013001039>
- 1165 [47] D. J. Segalman, M. S. Allen, M. Eriten, K. Hoppman, Experimental Assessment of Joint-Like Modal Models for Structures, Vol. 8: 27th Conference on Mechanical Vibration and Noise of International Design Engineering Technical Conferences and Computers and Information in Engineering Conference, 2015 (2015). doi:<https://doi.org/10.1115/DETC2015-47946>.
1170
- [48] A. Fantetti, L. Tamatam, M. Volvert, I. Lawal, L. Liu, L. Salles, M. Brake, C. Schwingshackl, D. Nowell, The impact of fretting wear on structural dynamics: Experiment and simulation, *Tribology International* 138 (2019) 111–124 (2019).
1175 doi:<https://doi.org/10.1016/j.triboint.2019.05.023>.
URL <https://www.sciencedirect.com/science/article/pii/S0301679X19302828>
- [49] H. Jalali, H. Ahmadian, J. E. Mottershead, Identification of nonlinear bolted lap-joint parameters by force-state mapping, *International Journal of Solids and Structures* 44 (25) (2007) 8087 – 8105 (2007).
1180 doi:<https://doi.org/10.1016/j.ijsolstr.2007.06.003>.
URL <http://www.sciencedirect.com/science/article/pii/S0020768307002417>